SUPPLEMENTARY MATERIAL

Article title: Comparative LC-MS/MS profiling of molecular features in Antarctic bacteria

Journal: Applied Microbiology and Biotechnology

Authors: José Aparecido Ferreira de Lima[2], Paulo Henrique Lima[1,3], Daniel Carvalho Pimenta[2], Alexandre Soares Rosado[4], Adalberto Pessoa[3]

Author affiliations: [1] Laboratory of Pharmacology, Butantan Institute, São Paulo, SP, Brazil; [2] Laboratory of Ecology and Evolution, Butantan Institute, São Paulo, SP, Brazil; [3] Biochemical-Pharmaceutical Technology, School of Pharmaceutical Sciences, University of São Paulo, São Paulo, SP, Brazil; [4] Biological and Environmental Sciences and Engineering (BESE), King Abdullah University of Science and Technology (KAUST), Thuwal, Kingdom of Saudi Arabia

Corresponding author:

Paulo Henrique Lima

Email: paulo.henrique@fundacaobutantan.org.br

Fig. S1 Photodiode array (PDA) contour plot of the G1 bacterial strain extract, showing absorbance as a function of retention time and wavelength

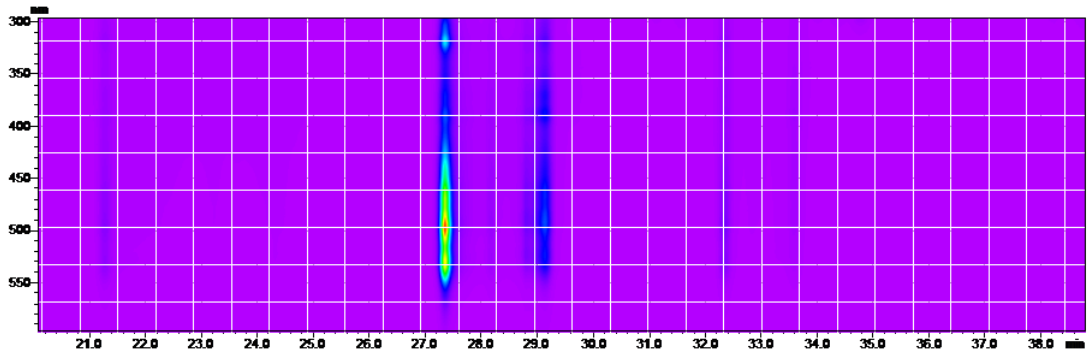


Fig. S2 Chromatographic profile of the G1 bacterial strain extract, showing the chromatographic signal as a function of retention time together with the programmed gradient of mobile phase B

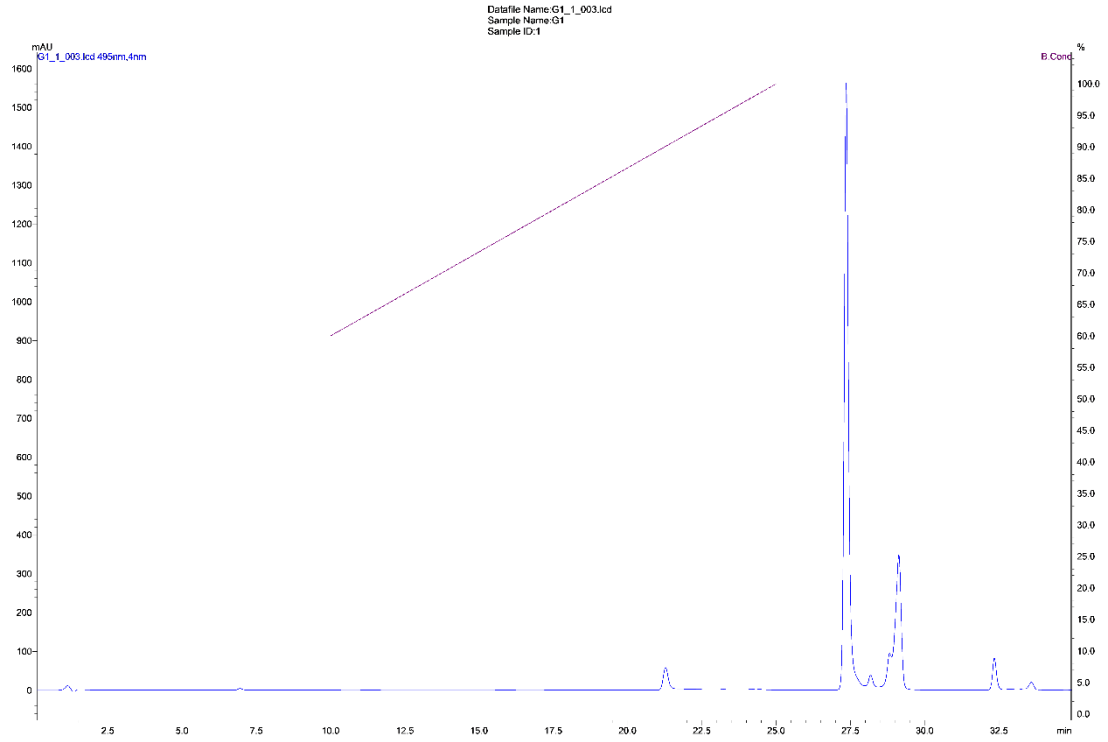


Fig. S3 Low-resolution mass spectrum of the G1 bacterial strain extract, showing the detected ions according to their mass-to-charge ratios (m/z) and relative intensities

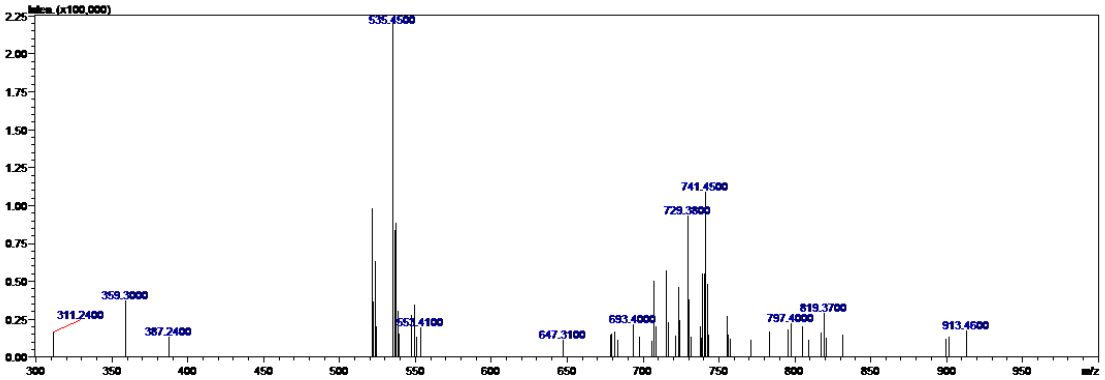


Fig. S4 High-resolution MS/MS spectrum of the precursor ion at m/z 628.3714 detected in the G1 bacterial strain extract, showing product ions at m/z 551.5013, 398.2324, and 313.2724

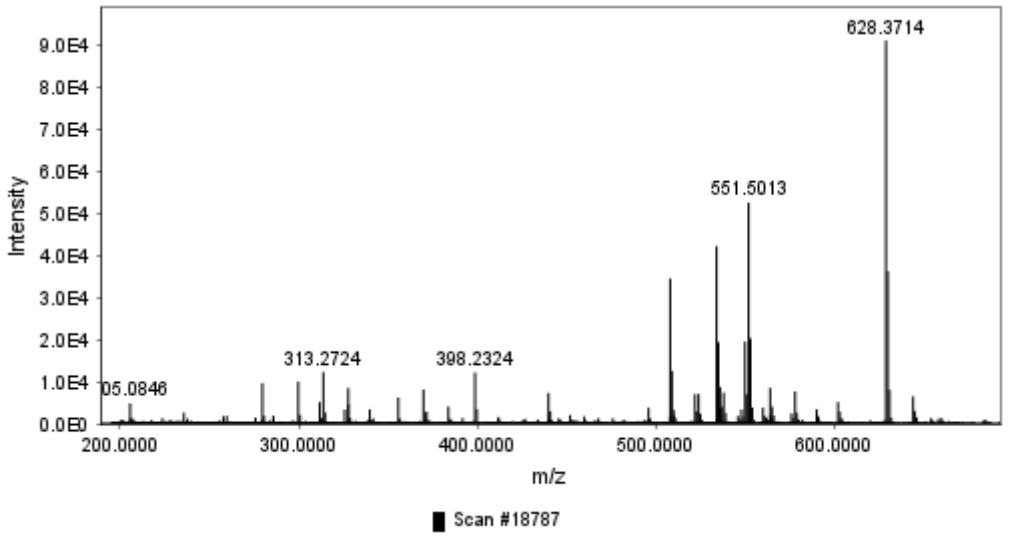


Fig. S5 High-resolution MS/MS spectrum of the precursor ion at m/z 563.5021 detected in the G1 bacterial strain extract, showing product ions at m/z 411.3984 and 313.2730

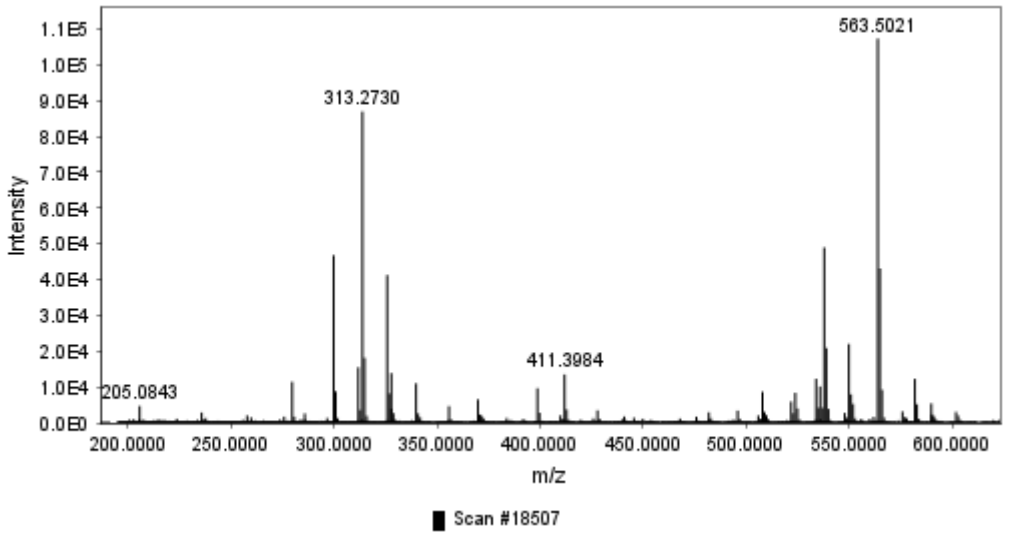


Fig. S6 High-resolution MS/MS spectrum of the precursor ion at m/z 549.4854 detected in the G1 bacterial strain extract, showing product ions at m/z 398.2325 and 313.2727

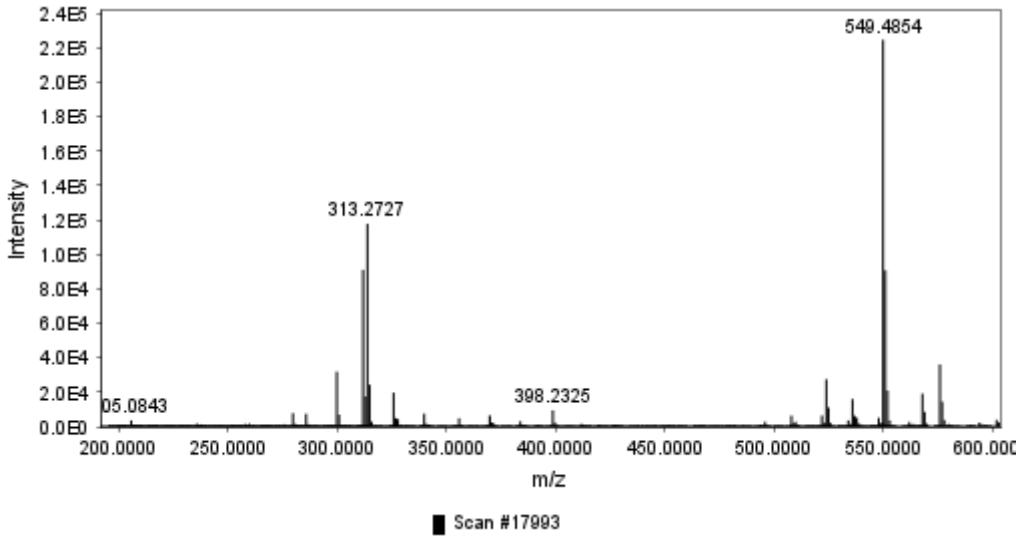


Fig. S7 High-resolution MS/MS spectrum of the precursor ion at m/z 523.4704 detected in the G1 bacterial strain extract, showing product ions at m/z 431.3882, 369.3721, and 299.2573

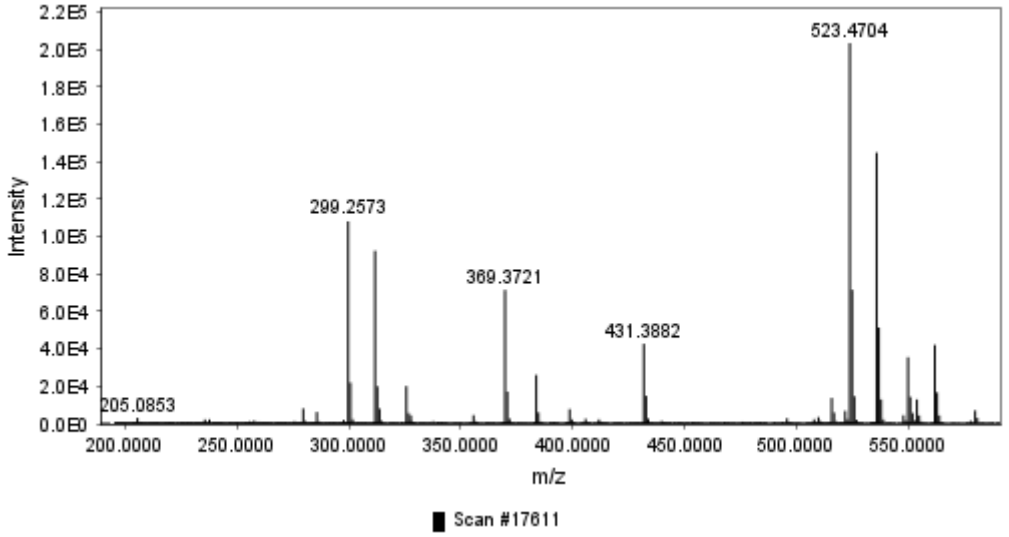


Fig. S8 High-resolution MS/MS spectrum of the precursor ion at m/z 547.4692 detected in the G1 bacterial strain extract, showing product ions at m/z 311.2570 and 398.2316

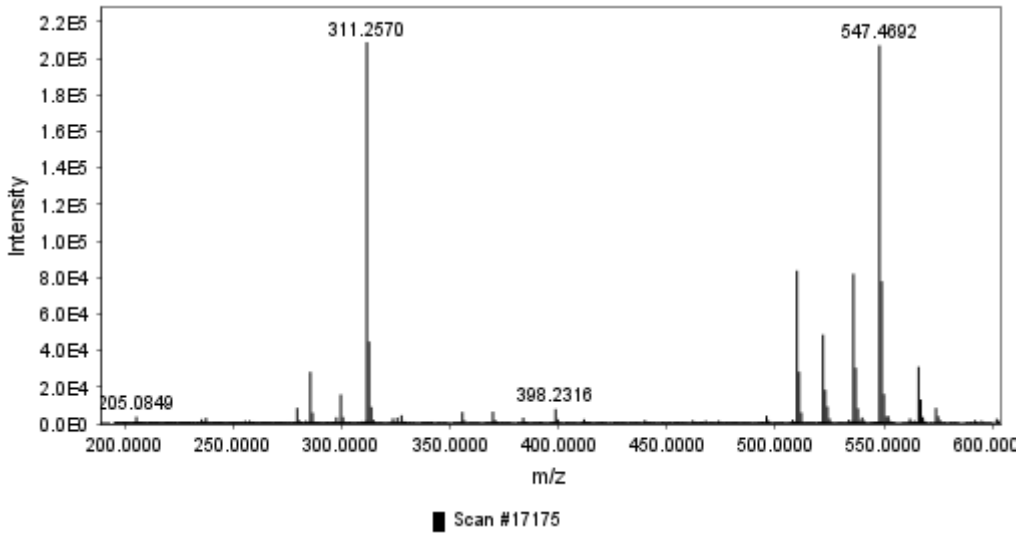


Fig. S9 High-resolution MS/MS spectrum of the molecular feature at m/z 535.4700 detected in the G1 bacterial strain extract, showing product ions at m/z 447.3826, 369.3508, and 311.2571

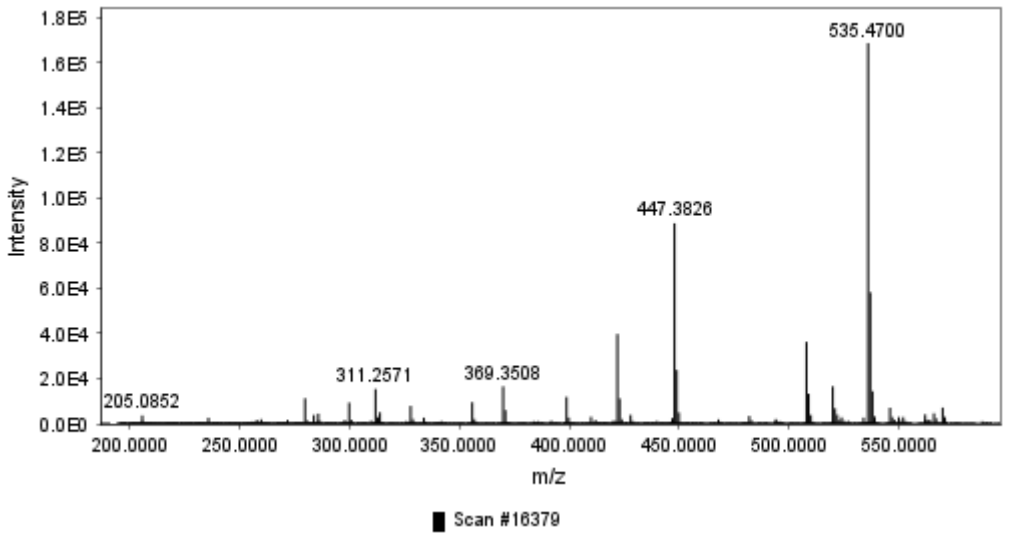


Fig. S10 High-resolution MS/MS spectrum of the precursor ion at m/z 417.3358 detected in the G1 bacterial strain extract, showing product ions at m/z 379.3198, 313.2727, 279.1577, and 235.2045

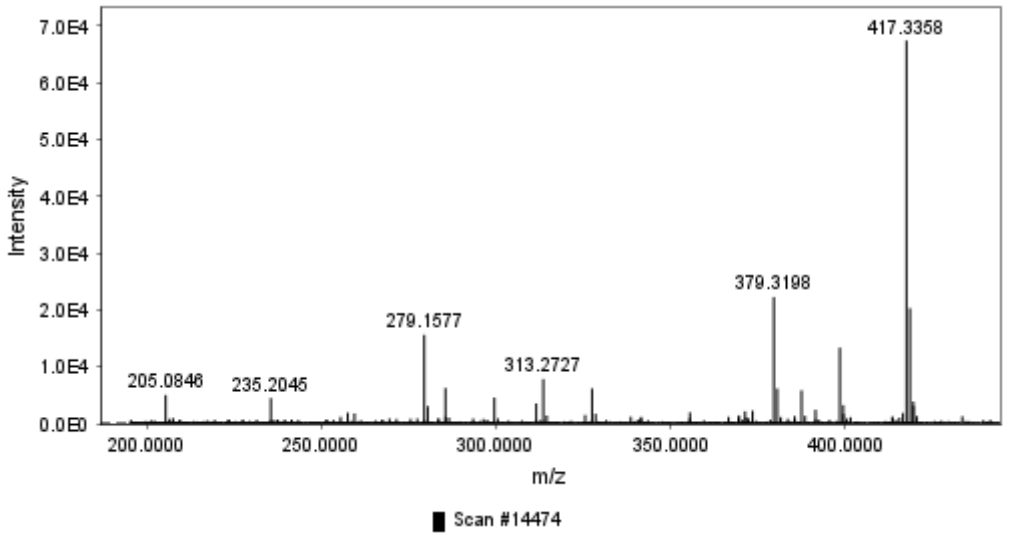


Fig. S11 High-resolution MS/MS spectrum of the precursor ion at m/z 521.4548 detected in the G1 bacterial strain extract, showing product ions at m/z 439.3774, 387.2738, 327.2520, and 279.1579

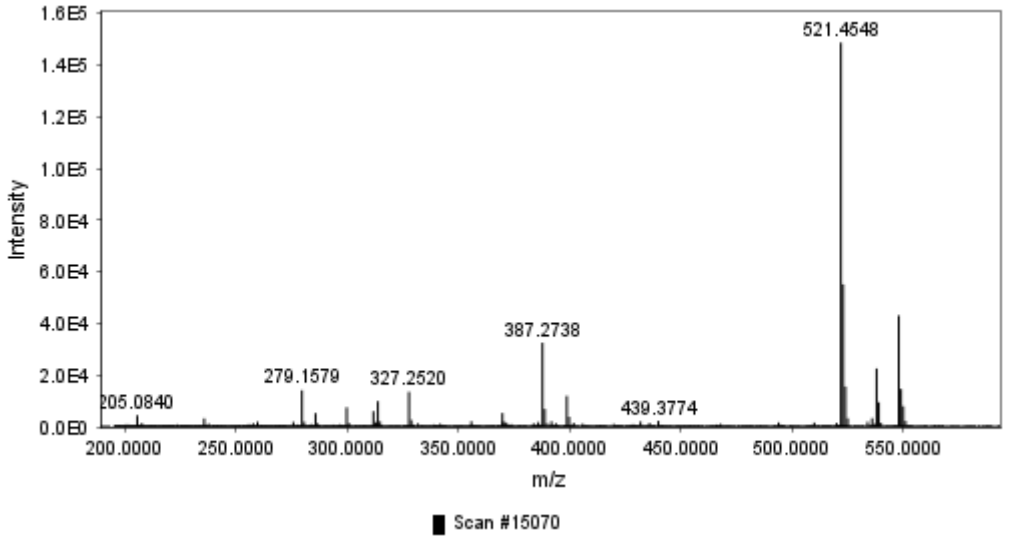


Fig. S12 High-resolution MS/MS spectrum of the molecular feature at m/z 741.5786 detected in the G1 bacterial strain extract, showing a prominent product-ion signal at m/z 338.3409. The molecular identity of the precursor remains unresolved

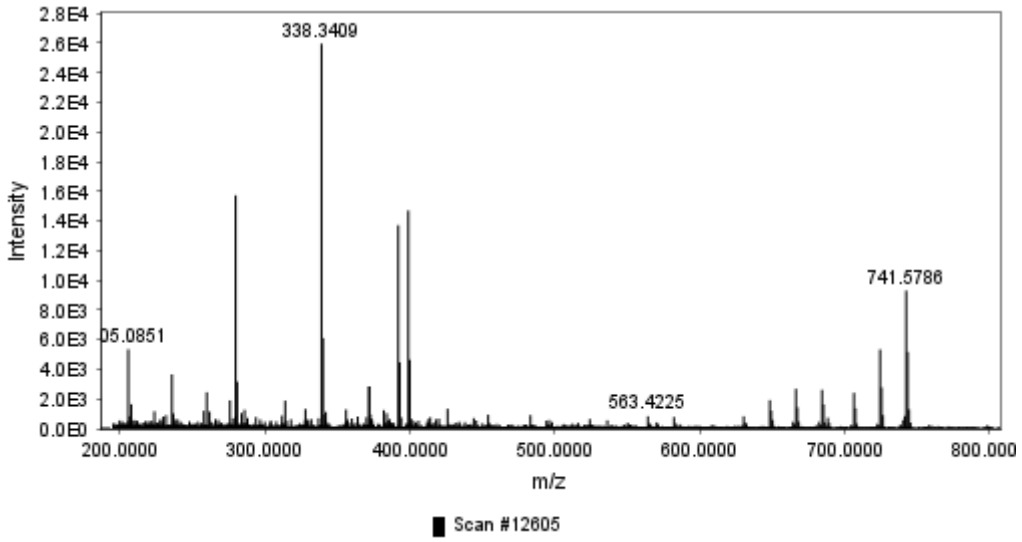


Fig. S13 Photodiode array (PDA) contour plot of the B1 bacterial strain extract, showing absorbance as a function of retention time and wavelength

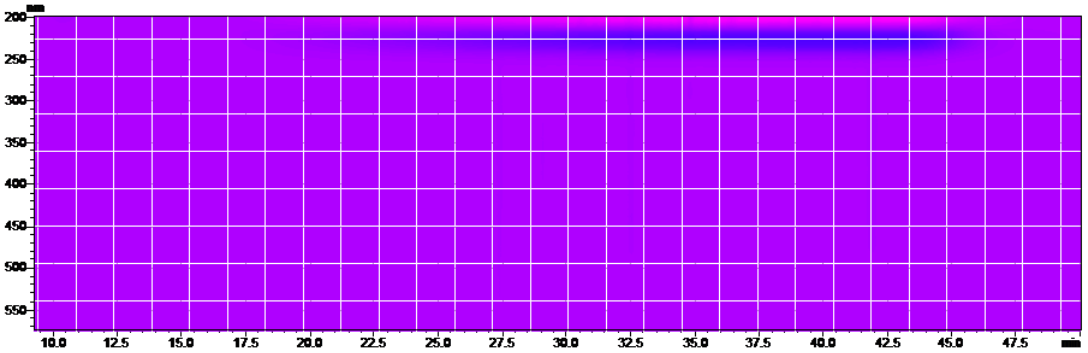


Fig. S14 Chromatographic profile of the B1 bacterial strain extract, showing the chromatographic signal as a function of retention time together with the programmed gradient of mobile phase B

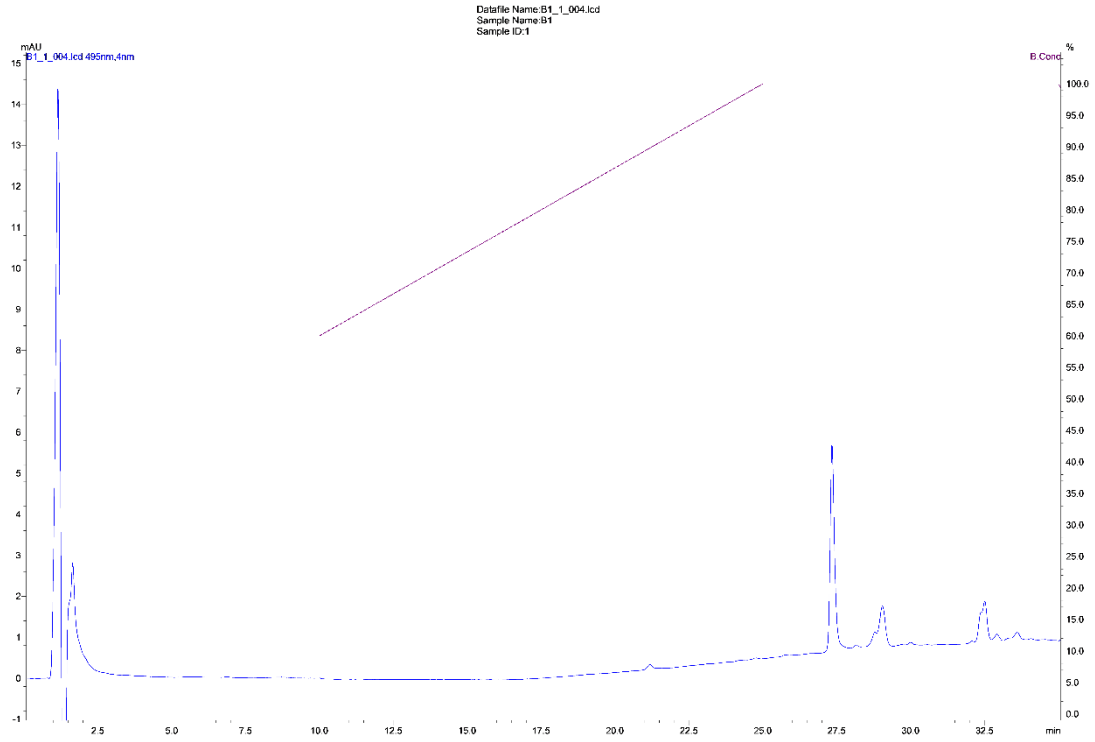


Fig. S15 Low-resolution mass spectrum of the B1 bacterial strain extract, showing the detected ions according to their m/z values and relative intensities

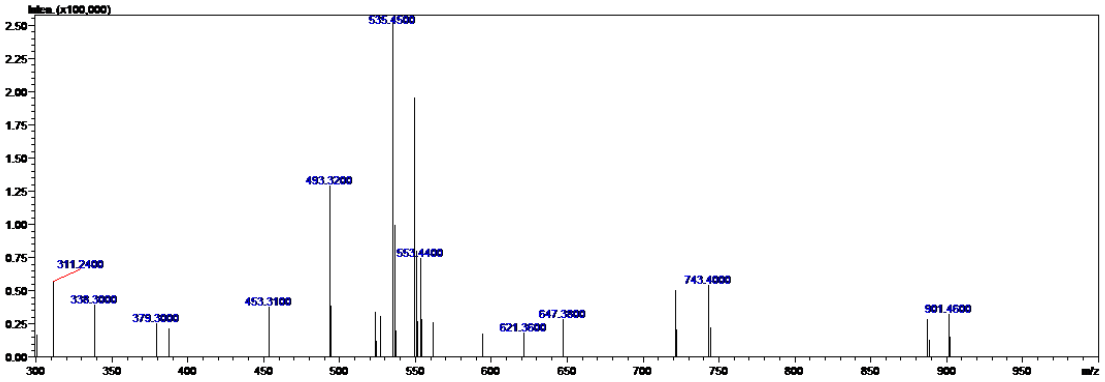


Fig. S16 High-resolution MS/MS spectrum of the precursor ion at m/z 551.5026 detected in the B1 bacterial strain extract, showing product ions at m/z 398.2320 and 299.2567

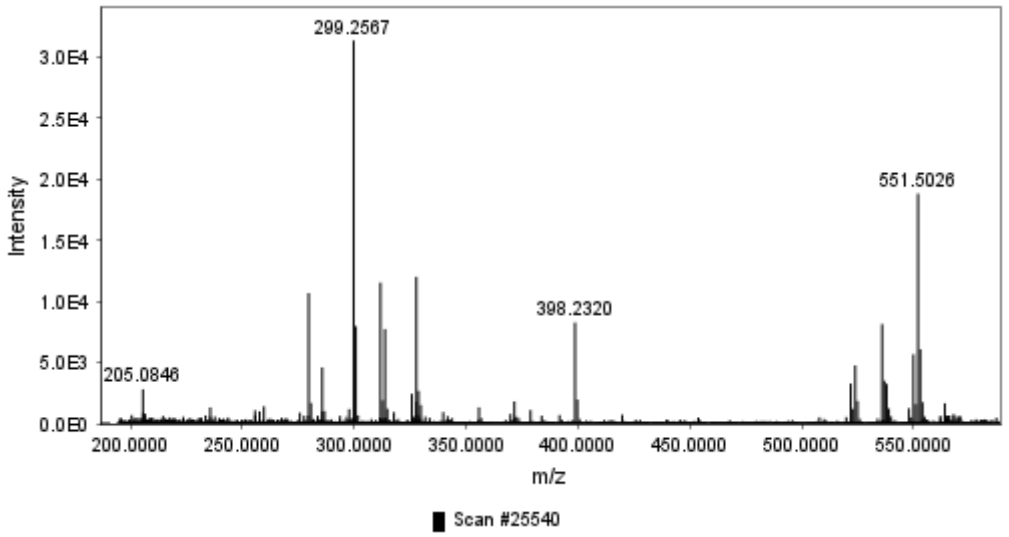


Fig. S17 High-resolution MS/MS spectrum of the precursor ion at m/z 579.5325 detected in the B1 bacterial strain extract, showing product ions at m/z 398.2326 and 279.1586

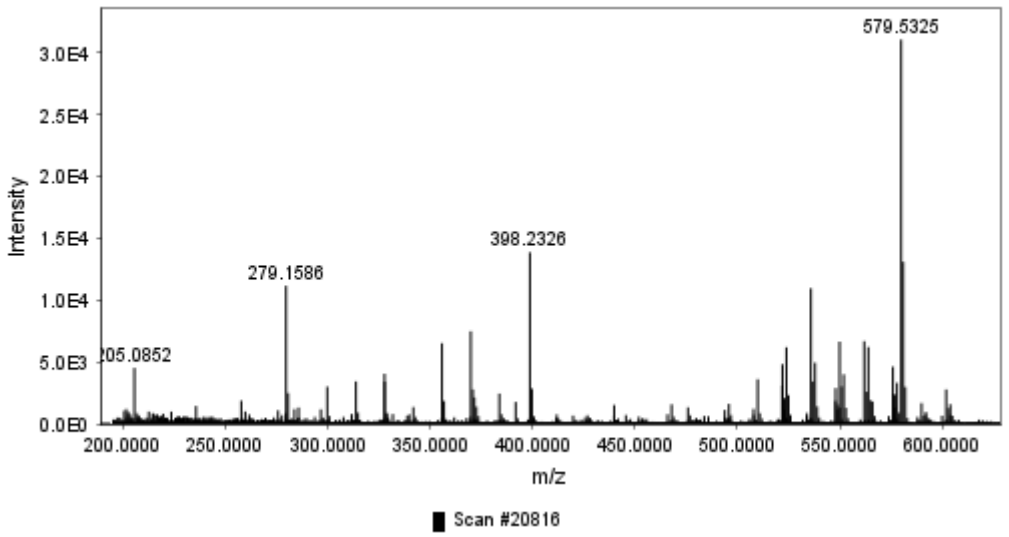


Fig. S18 High-resolution MS/MS spectrum of the precursor ion at m/z 537.4865 detected in the B1 bacterial strain extract, showing product ions at m/z 411.3988, 369.3515, and 313.2729

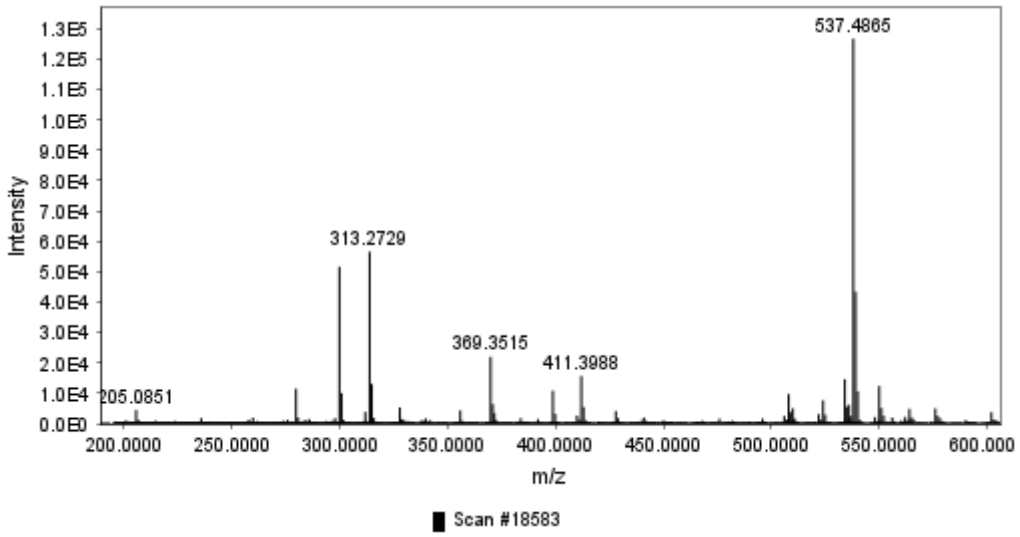


Fig. S19 High-resolution MS/MS spectrum of the precursor ion at m/z 549.4851 detected in the B1 bacterial strain extract, showing product ions at m/z 369.3514 and 299.2568

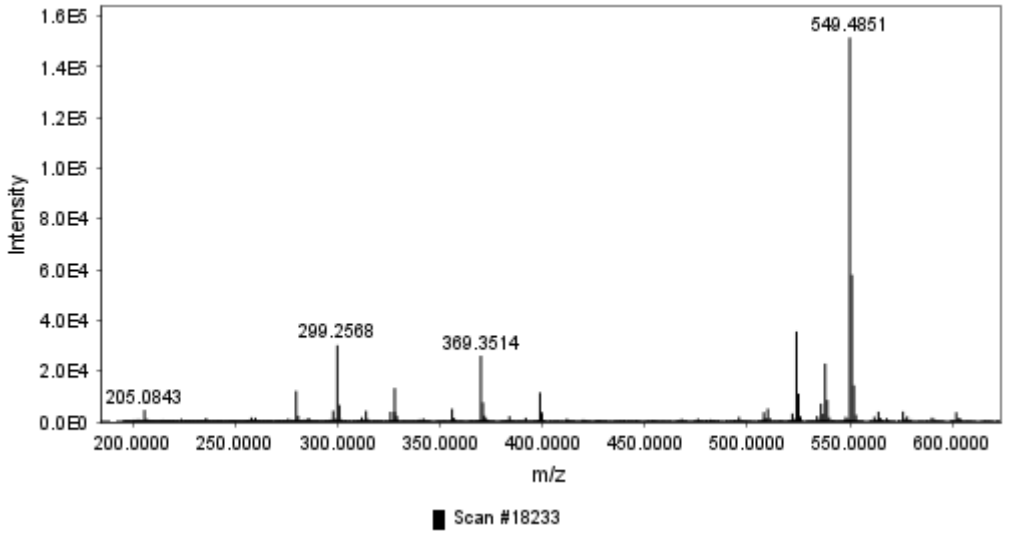


Fig. S20 High-resolution MS/MS spectrum of the precursor ion at m/z 523.4700 detected in the B1 bacterial strain extract, showing product ions at m/z 369.3669 and 299.2569

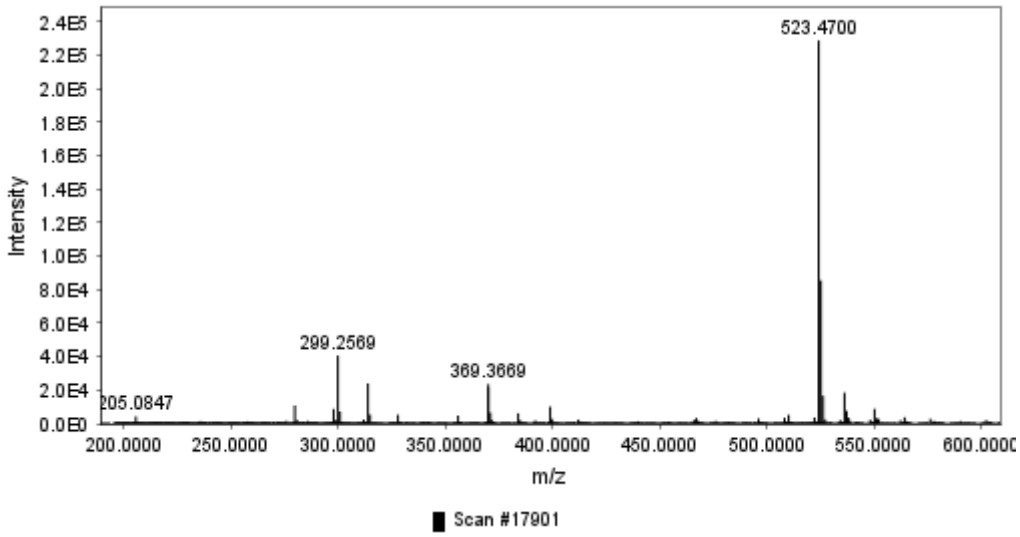


Fig. S21 High-resolution MS/MS spectrum of the precursor ion at m/z 521.4546 detected in the B1 bacterial strain extract, showing product ions at m/z 369.3507 and 299.2569

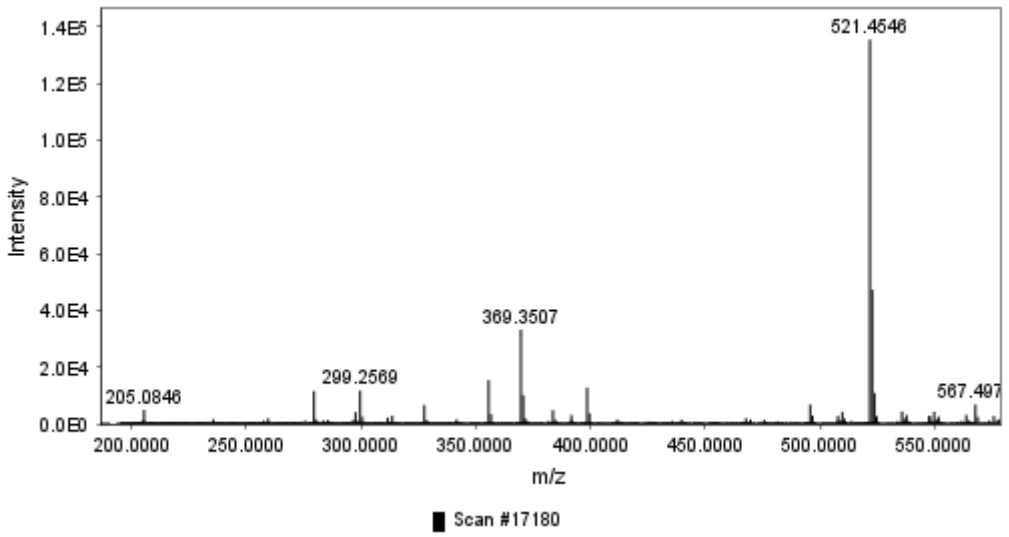


Fig. S22 High-resolution MS/MS spectrum of the precursor ion at m/z 509.4549 detected in the B1 bacterial strain extract, showing product ions at m/z 369.3510 and 299.2568

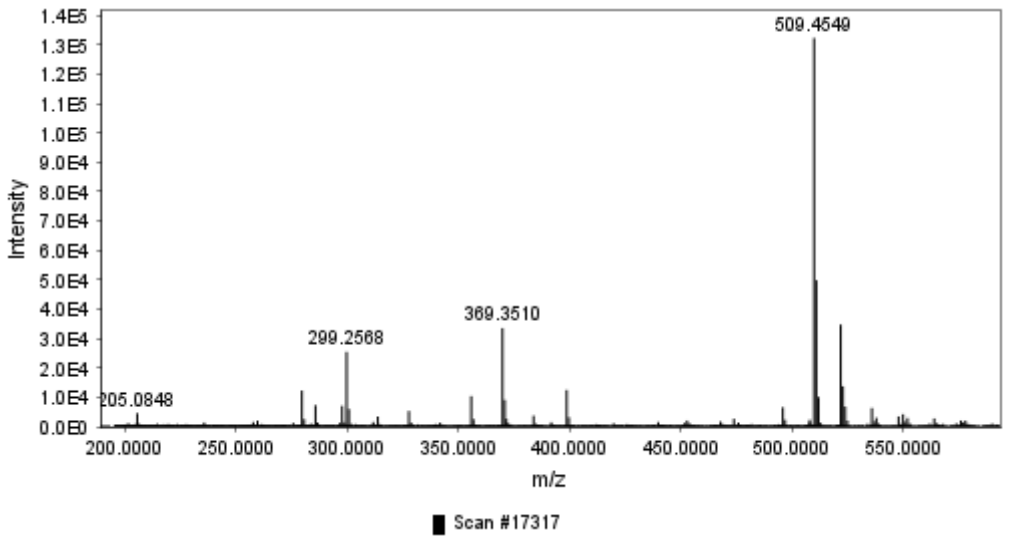


Fig. S23 High-resolution MS/MS spectrum of the precursor ion at m/z 713.5516 detected in the B1 bacterial strain extract, showing product ions at m/z 531.4064, 387.2735, and 279.1583

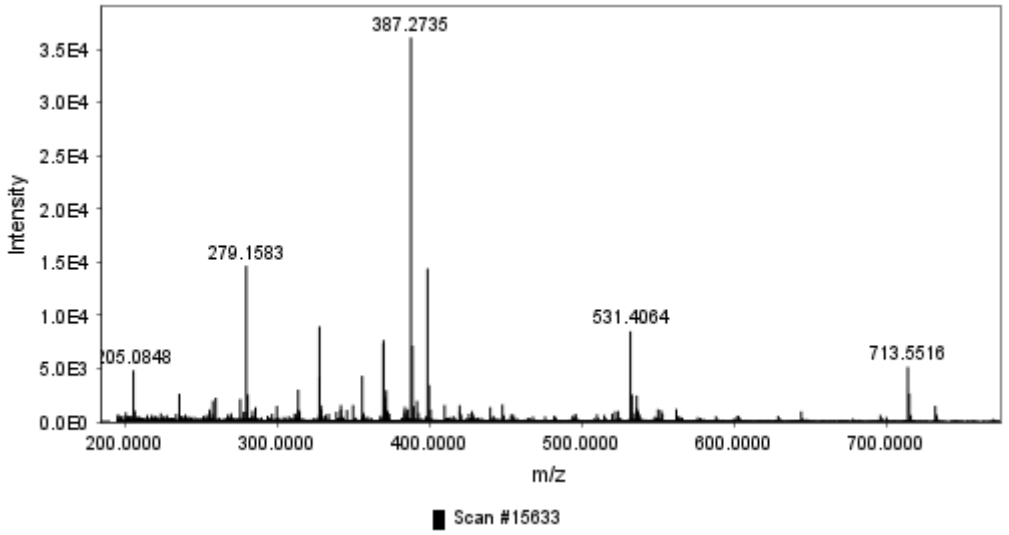


Fig. S24 High-resolution MS/MS spectrum of the precursor ion at m/z 685.5205 detected in the B1 bacterial strain extract, showing product ions at m/z 523.4707, 387.2735, and 279.1579

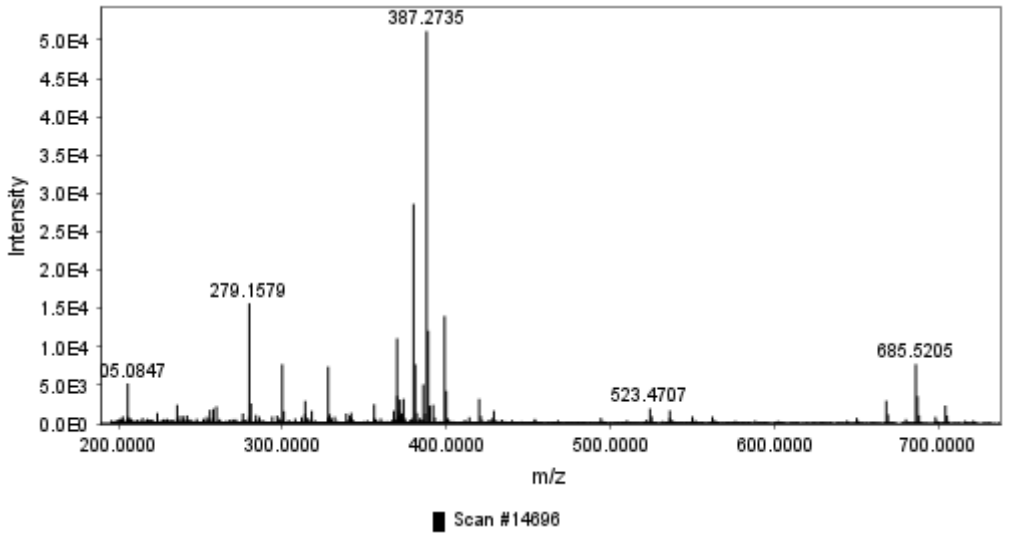


Fig. S25 High-resolution MS/MS spectrum of the precursor ion at m/z 699.5373 detected in the B1 bacterial strain extract, showing product ions at m/z 279.1582, 387.2735, 464.3524, and 535.5436

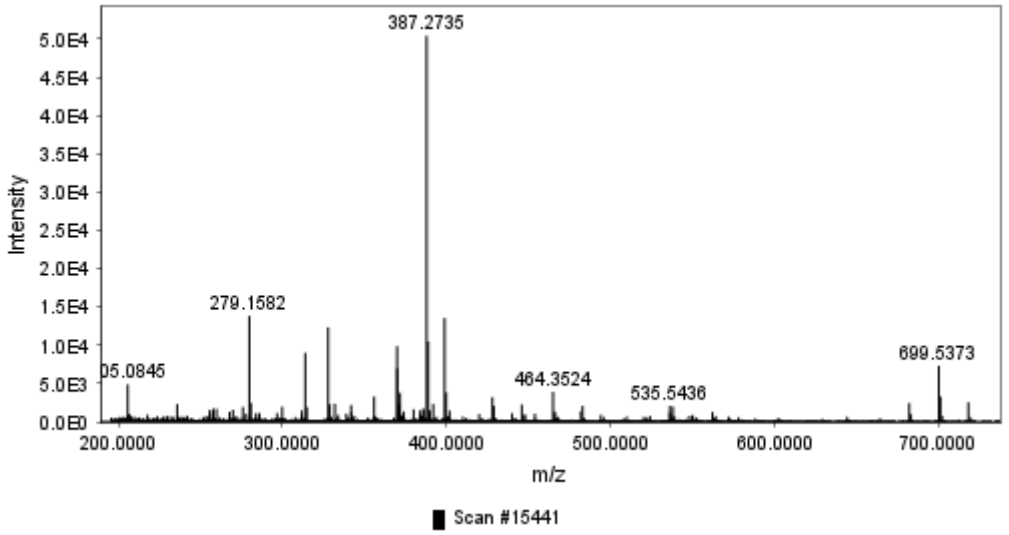


Fig. S26 Photodiode array (PDA) contour plot of the C7 bacterial strain extract, showing absorbance as a function of retention time and wavelength

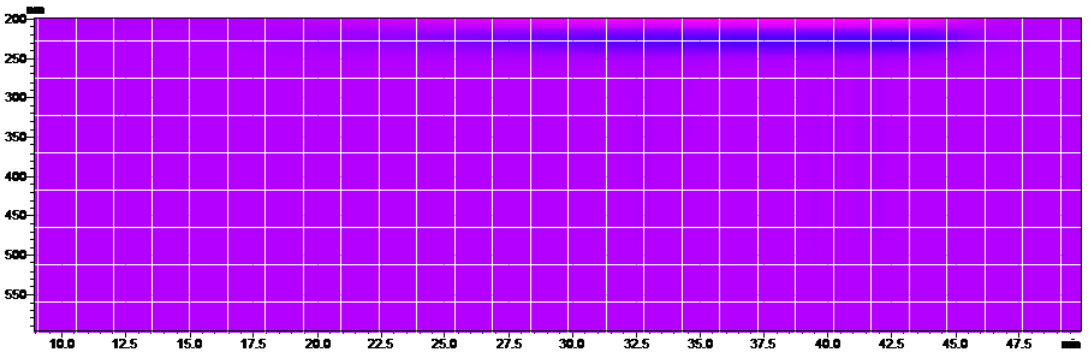


Fig. S27 Chromatographic profile of the C7 bacterial strain extract, showing the chromatographic signal as a function of retention time together with the programmed gradient of mobile phase B

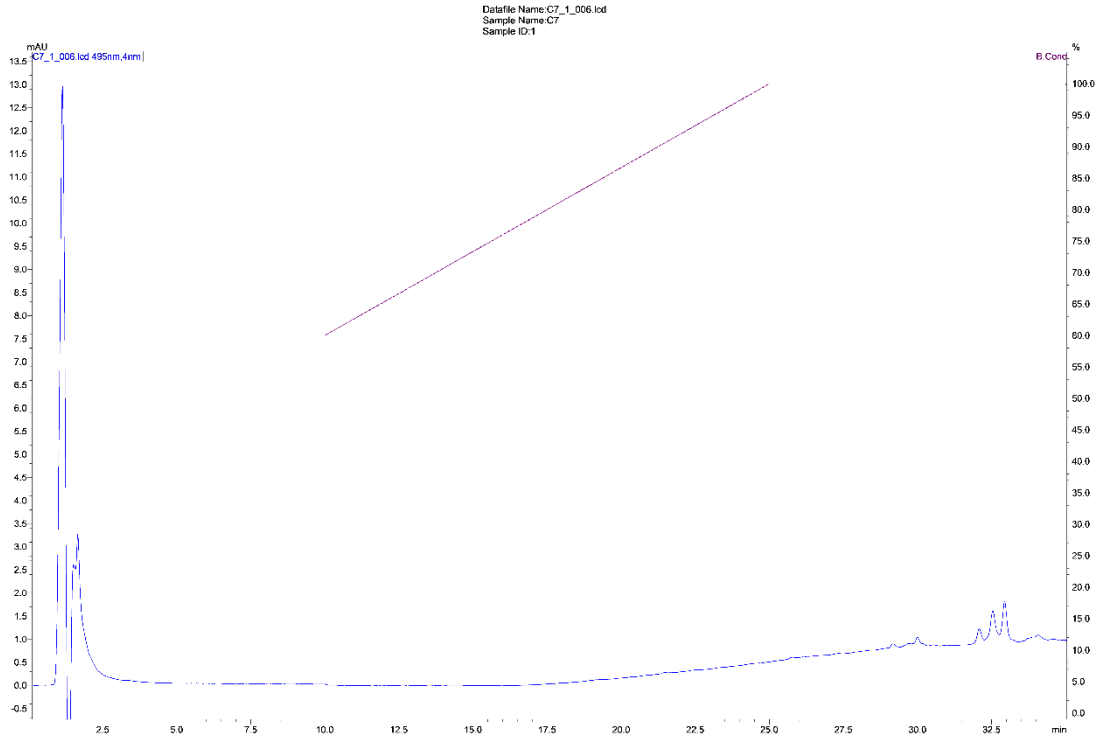


Fig. S28 Low-resolution mass spectrum of the C7 bacterial strain extract, showing the detected ions according to their m/z values and relative intensities

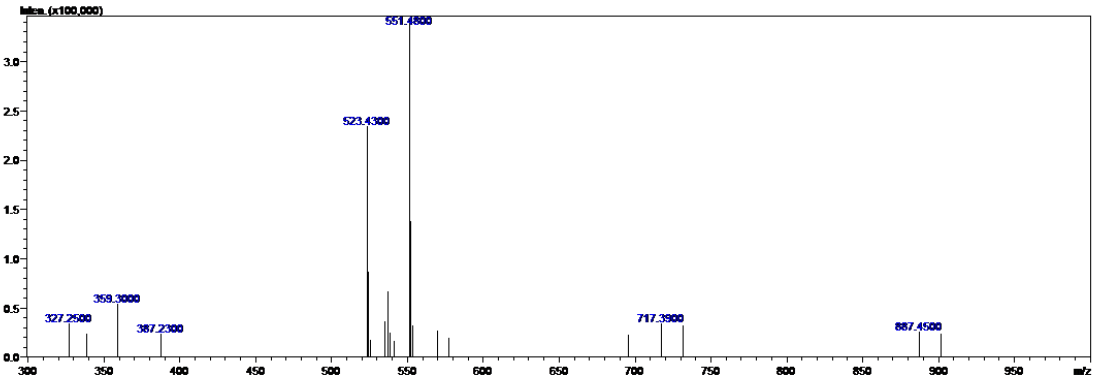


Fig. S29 High-resolution MS/MS spectrum of the precursor ion at m/z 551.5006 detected in the C7 bacterial strain extract, showing a product ion at m/z 327.2885

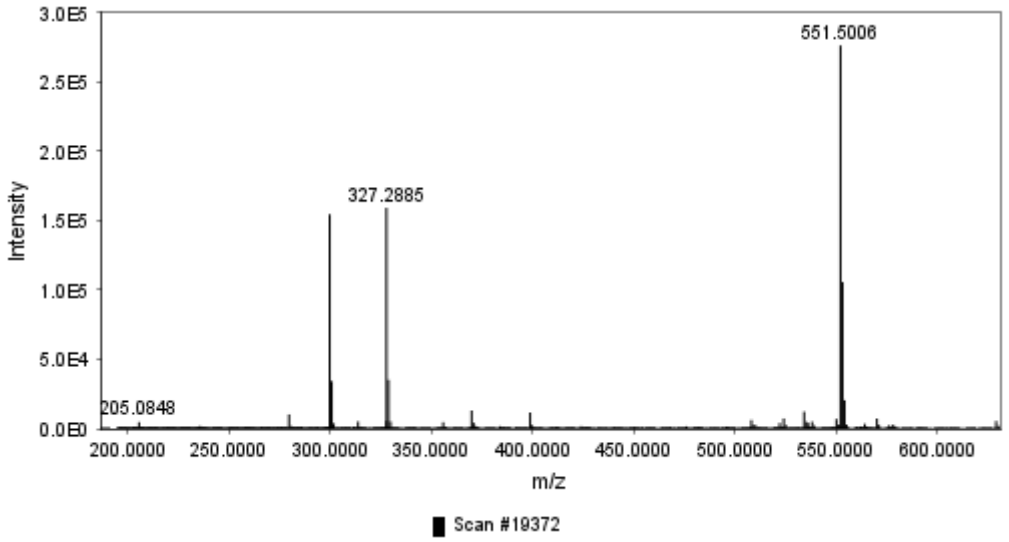


Fig. S30 High-resolution MS/MS spectrum of the precursor ion at m/z 537.4859 detected in the C7 bacterial strain extract, showing product ions at m/z 398.2323 and 313.2727

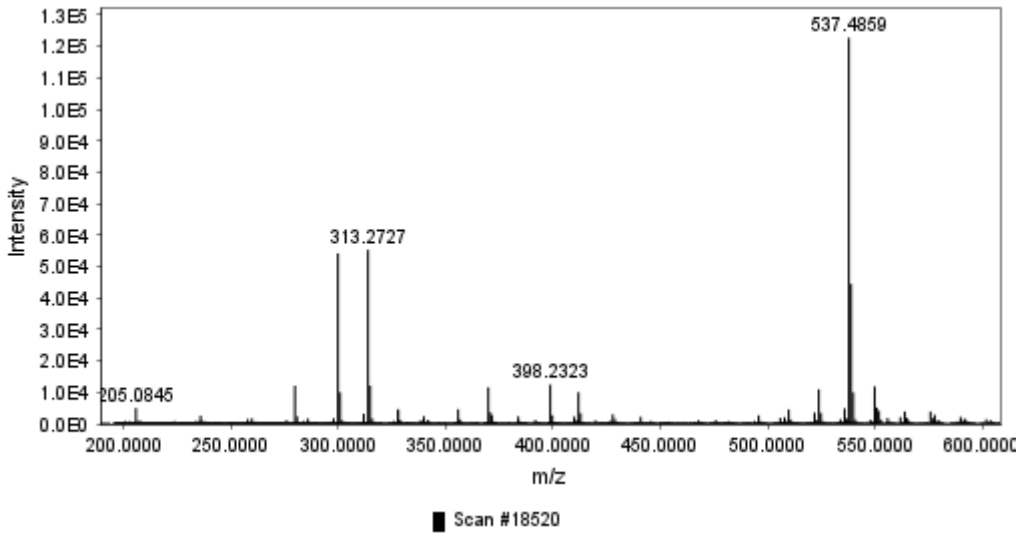


Fig. S31 High-resolution MS/MS spectrum of the precursor ion at m/z 549.4864 detected in the C7 bacterial strain extract, showing product ions at m/z 369.3529 and 299.2575

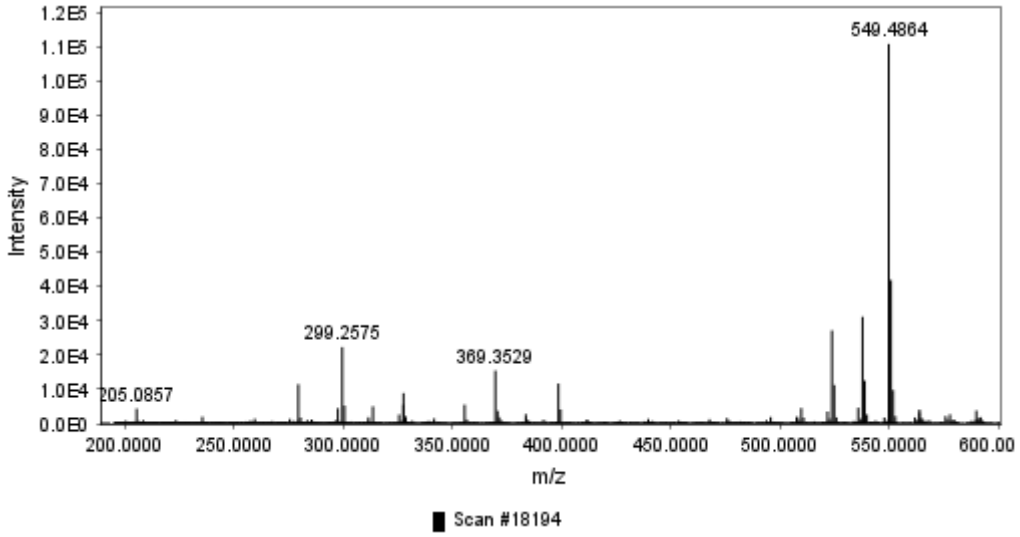


Fig. S32 High-resolution MS/MS spectrum of the precursor ion at m/z 523.4707 detected in the C7 bacterial strain extract, showing product ions at m/z 439.3786, 398.2326, and 299.2571

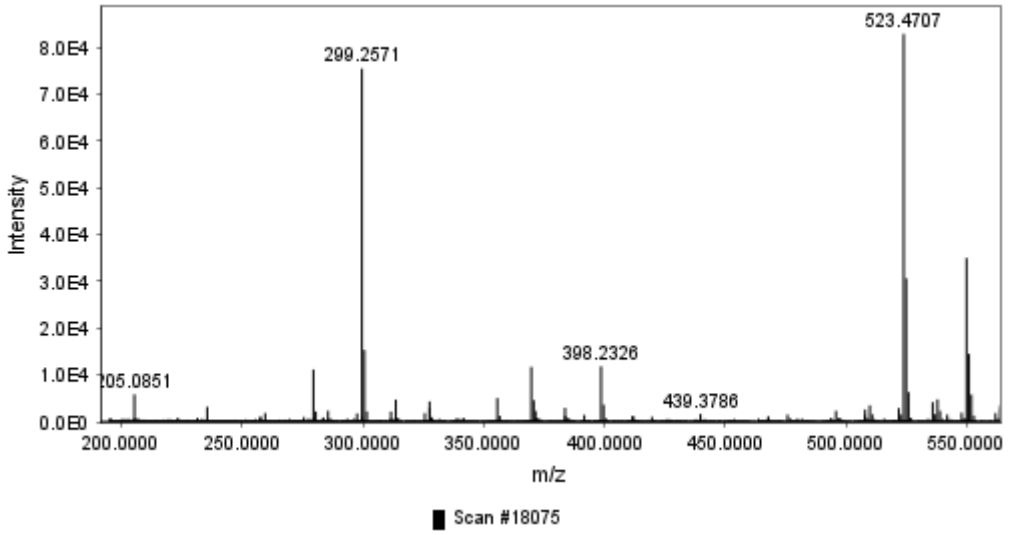


Fig. S33 High-resolution MS/MS spectrum of the molecular feature at m/z 535.4706 detected in the C7 bacterial strain extract, showing product ions at m/z 369.3508 and 279.1580

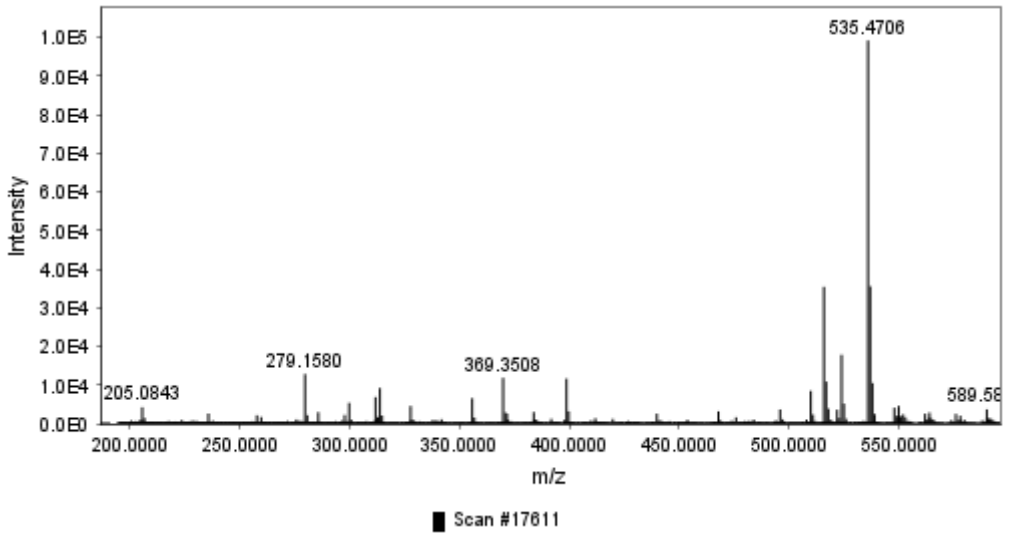


Fig. S34 High-resolution MS/MS spectrum of the precursor ion at m/z 509.4651 detected in the C7 bacterial strain extract, showing product ions at m/z 369.3512 and 299.2571

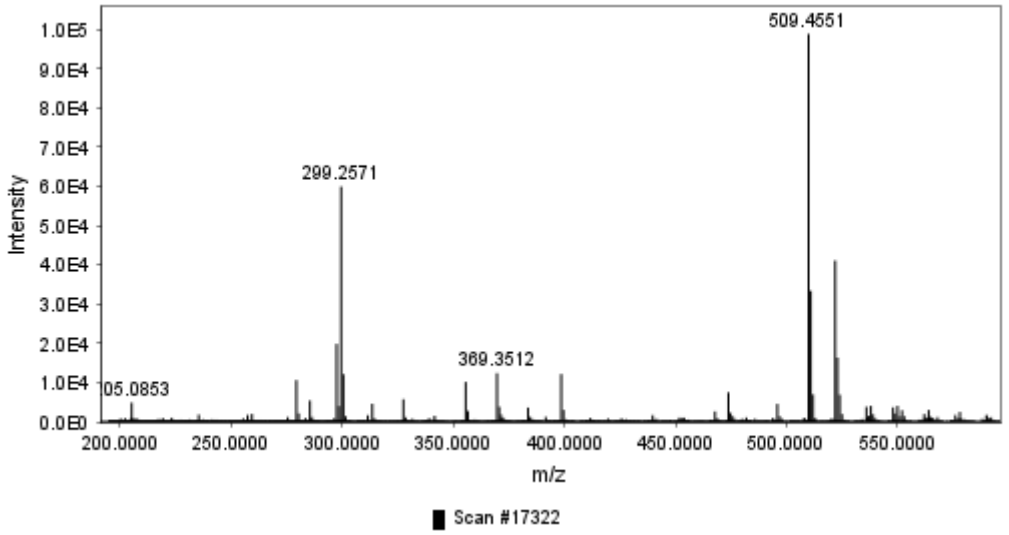


Fig. S35 High-resolution MS/MS spectrum of the precursor ion at m/z 713.5516 detected in the C7 bacterial strain extract, showing product ions at m/z 531.4060, 387.2741, and 279.1580

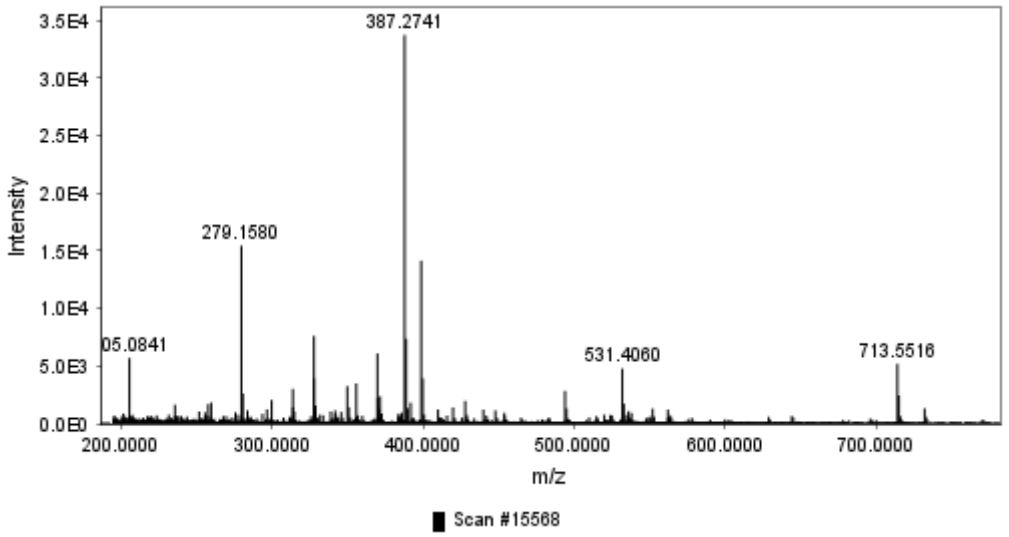


Fig. S36 High-resolution MS/MS spectrum of the precursor ion at m/z 699.5372 detected in the C7 bacterial strain extract, showing product ions at m/z 464.3518 and 387.2740

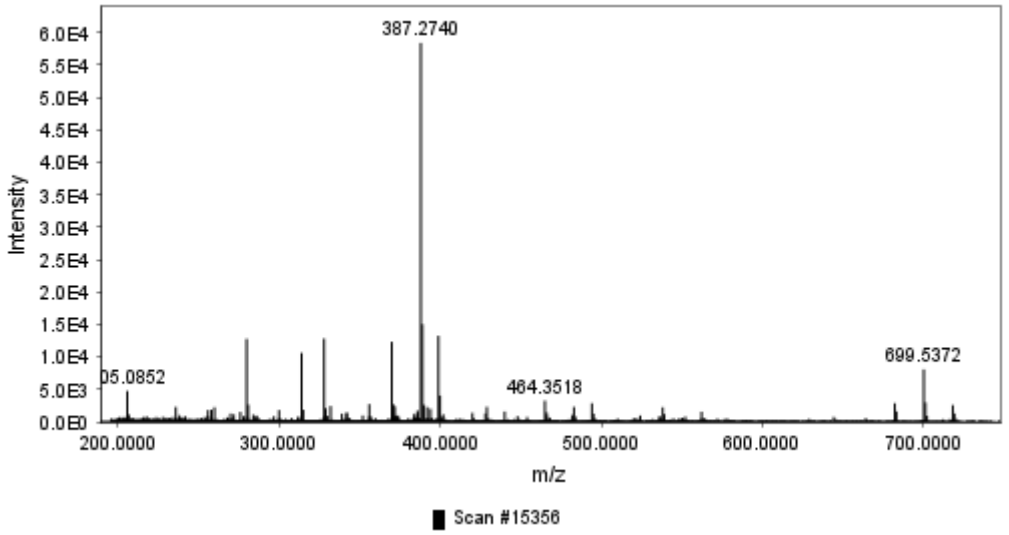


Fig. S37 High-resolution MS/MS spectrum of the precursor ion at m/z 685.5213 detected in the C7 bacterial strain extract, showing product ions at m/z 523.4711, 387.2736, and 279.1583

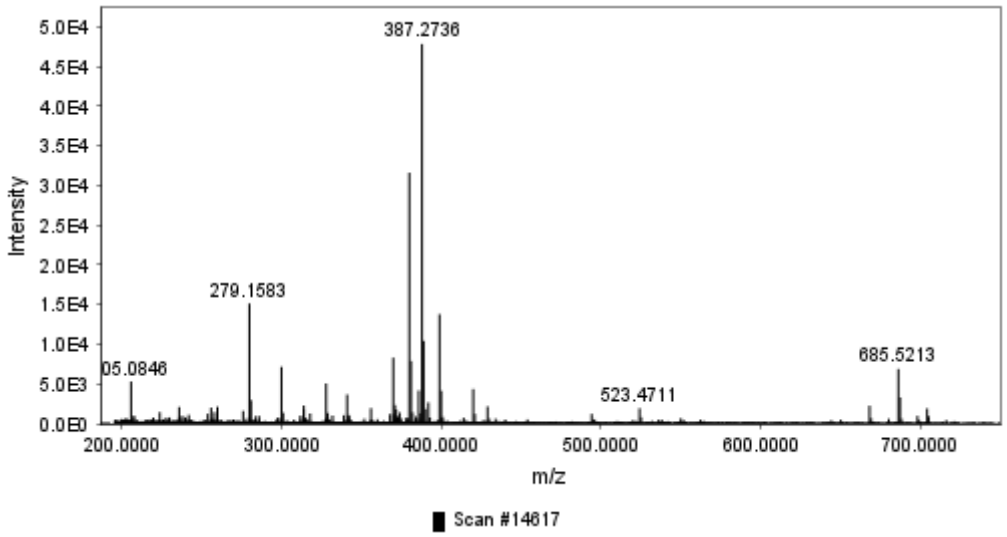


Fig. S38 Photodiode array (PDA) contour plot of the F1 bacterial strain extract, showing absorbance as a function of retention time and wavelength

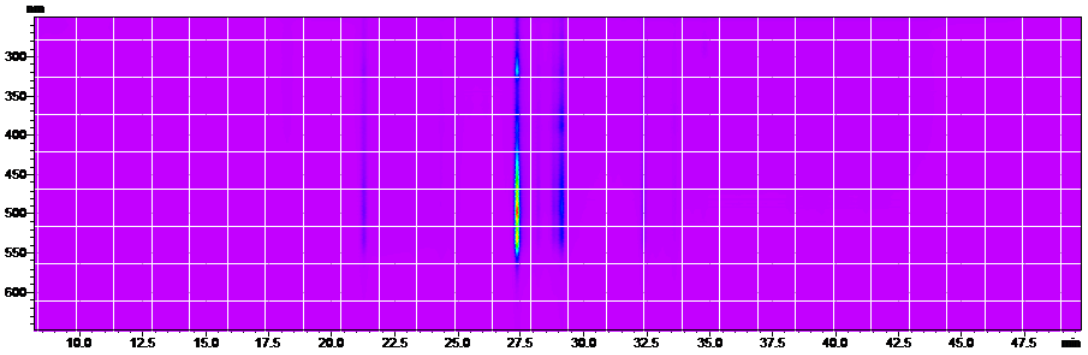


Fig. S39 Chromatographic profile of the F1 bacterial strain extract, showing the chromatographic signal as a function of retention time together with the programmed gradient of mobile phase B

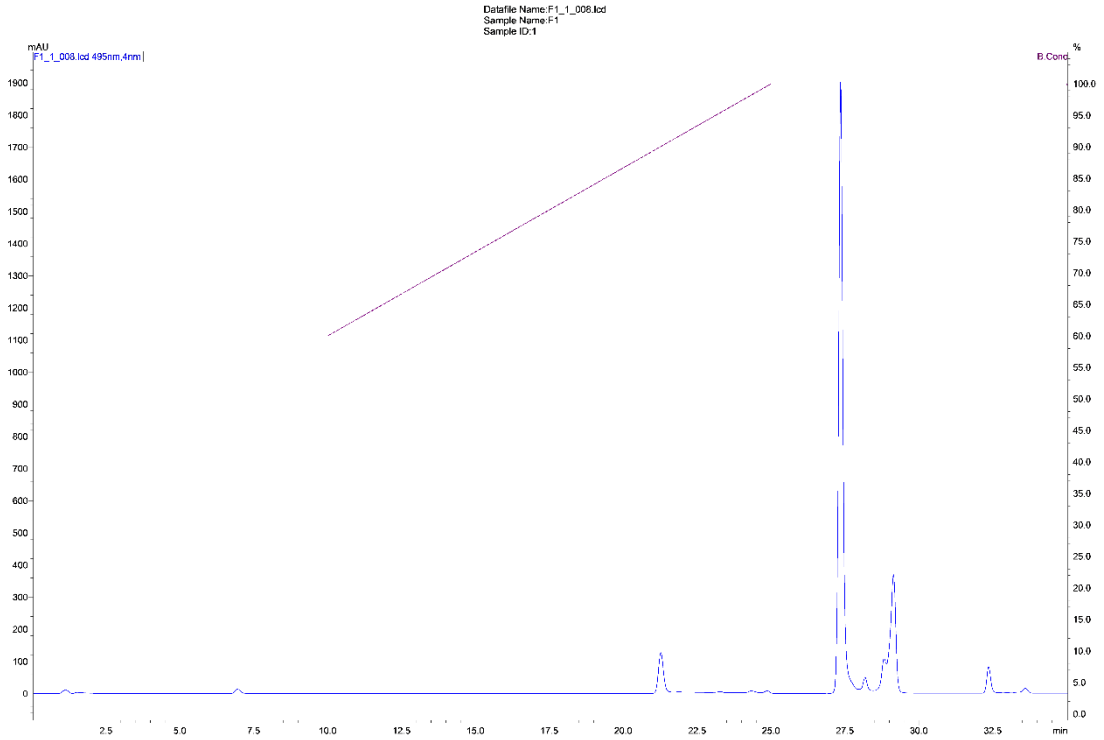


Fig. S40 Low-resolution mass spectrum of the F1 bacterial strain extract, showing the detected ions according to their m/z values and relative intensities

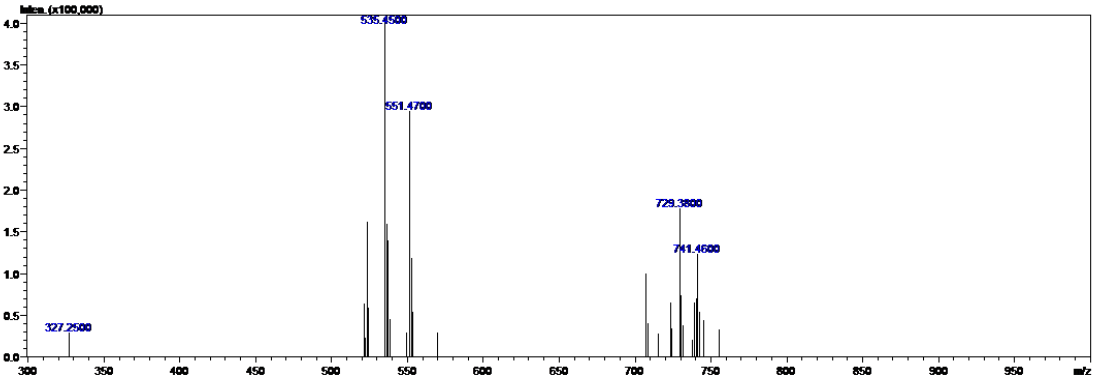


Fig. S41 High-resolution MS/MS spectrum of the precursor ion at m/z 577.5161 detected in the F1 bacterial strain extract, showing product ions at m/z 398.2320 and 313.2728

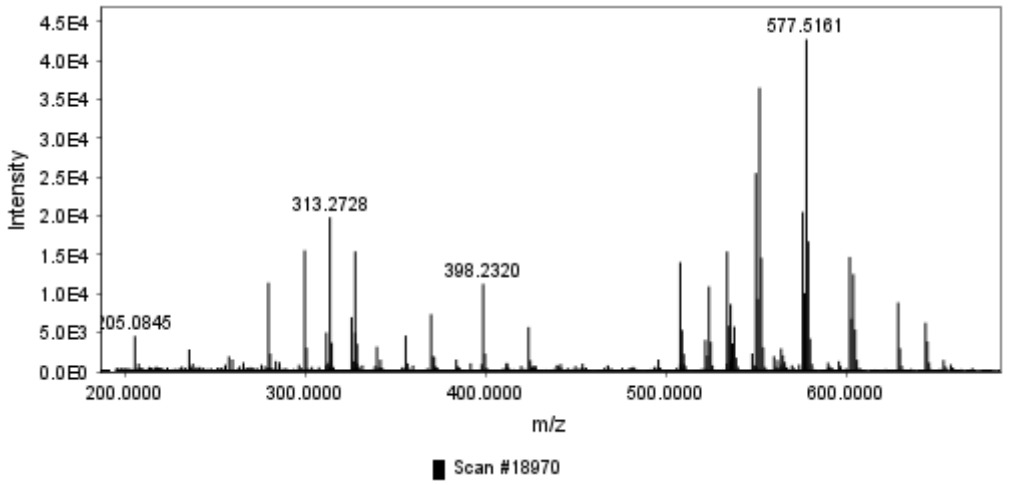


Fig. S42 High-resolution MS/MS spectrum of the precursor ion at m/z 628.3710 detected in the F1 bacterial strain extract, showing product ions at m/z 551.5006, 398.2323, and 299.2569

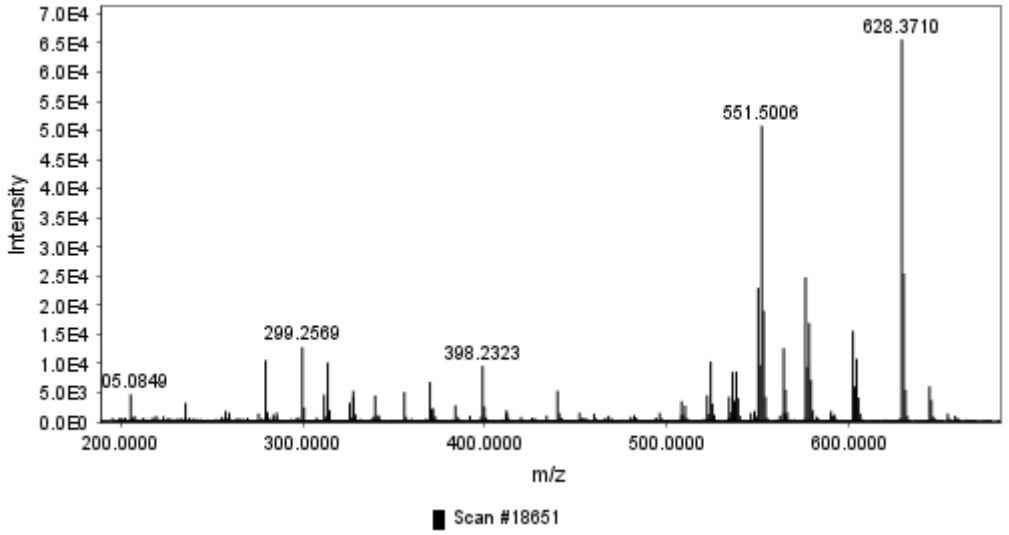


Fig. S43 High-resolution MS/MS spectrum of the precursor ion at m/z 537.4854 detected in the F1 bacterial strain extract, showing product ions at m/z 398.2319 and 313.2730

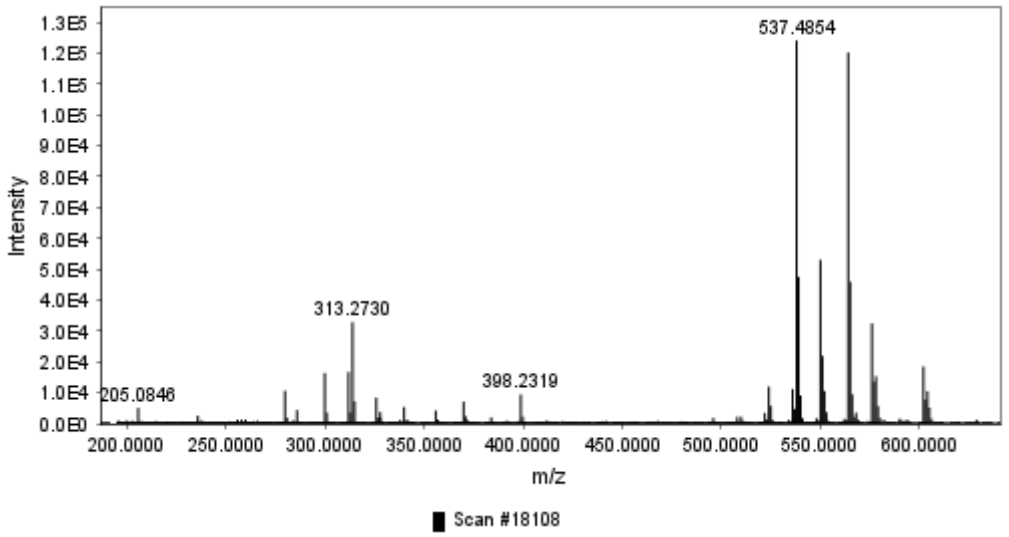


Fig. S44 High-resolution MS/MS spectrum of the precursor ion at m/z 535.4702 detected in the F1 bacterial strain extract, showing product ions at m/z 355.2838 and 433.3675

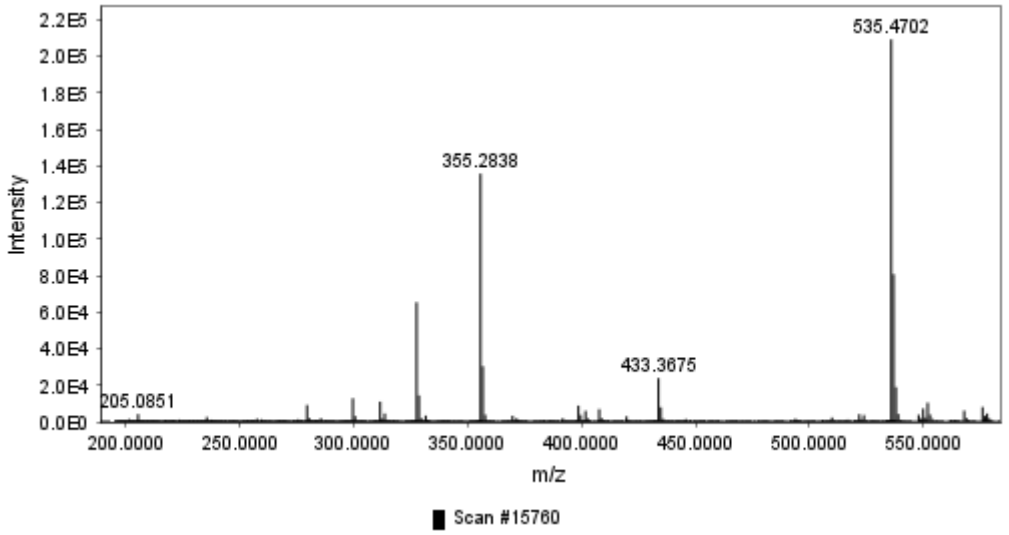


Fig. S45 High-resolution MS/MS spectrum of the precursor ion at m/z 447.3823 detected in the F1 bacterial strain extract, showing a product ion at m/z 311.2576

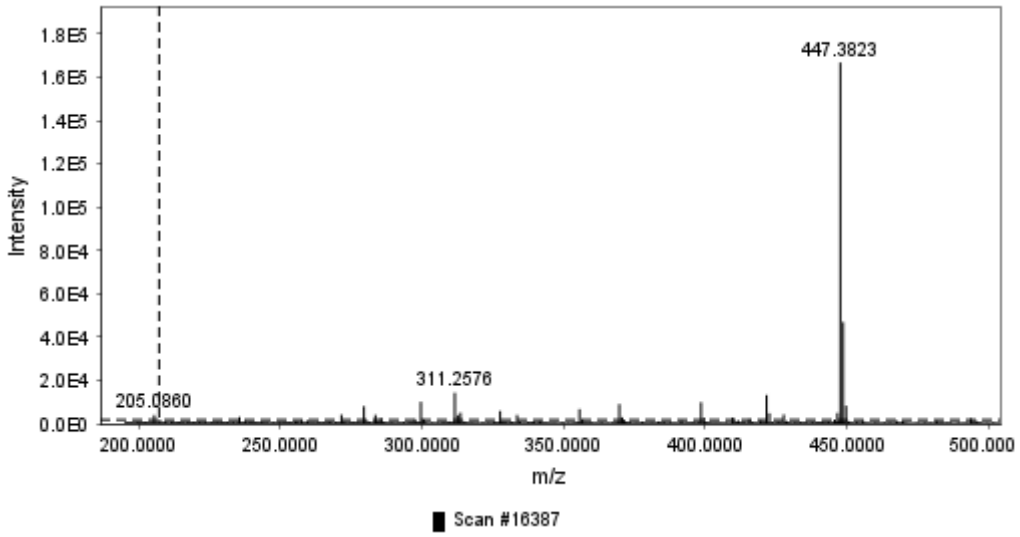


Fig. S46 High-resolution MS/MS spectrum of the molecular feature at m/z 535.4697 detected in the F1 bacterial strain extract, showing product ions at m/z 419.3506 and 279.1579

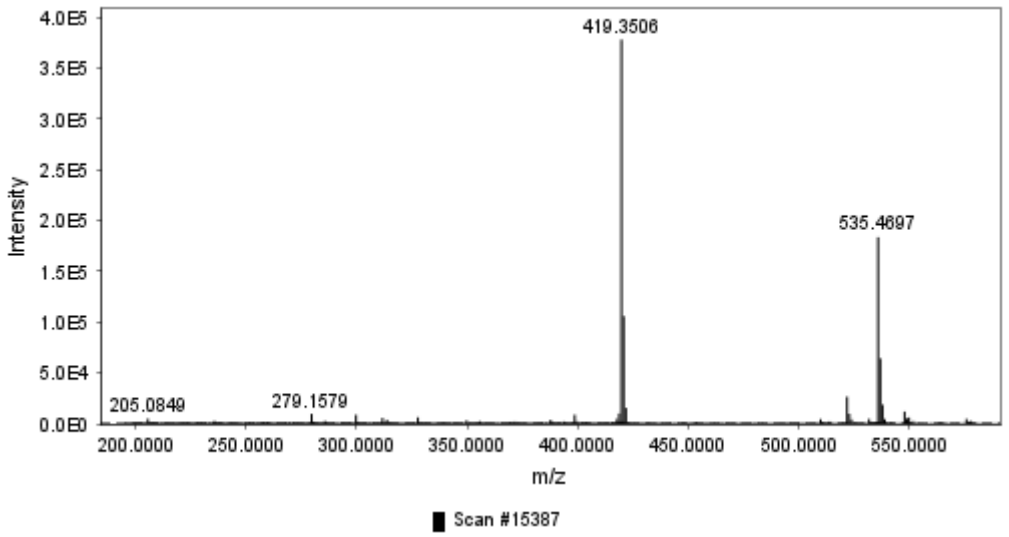


Fig. S47 High-resolution MS/MS spectrum of the precursor ion at m/z 521.4646 detected in the F1 bacterial strain extract, showing product ions at m/z 387.2732, 327.2517, and 279.1577

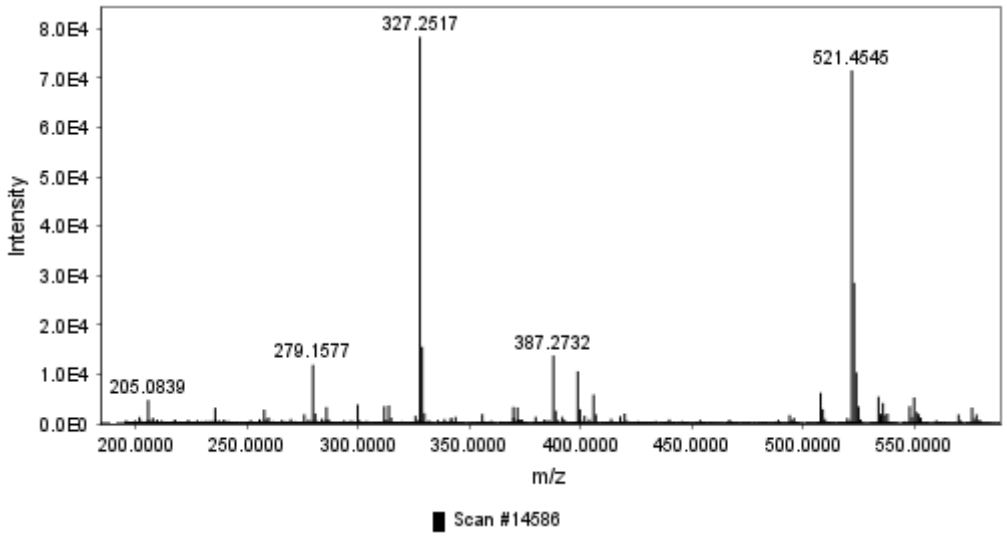


Fig. S48 Photodiode array (PDA) contour plot of the A1 bacterial strain extract, showing absorbance as a function of retention time and wavelength

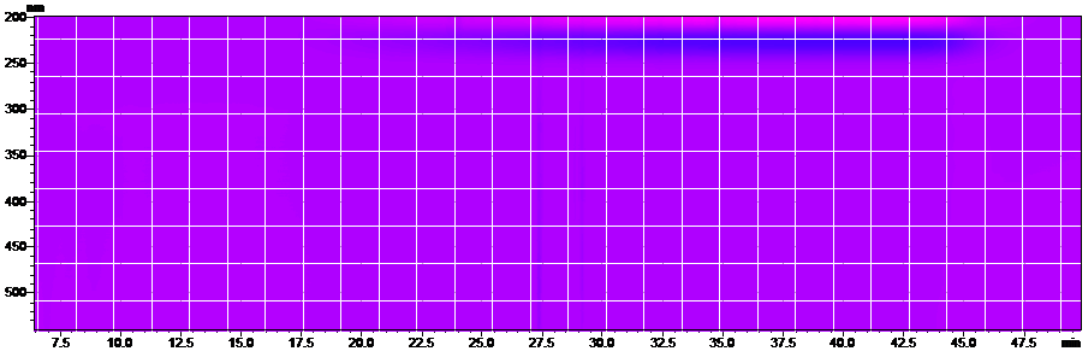


Fig. S49 Chromatographic profile of the A1 bacterial strain extract, showing the chromatographic signal as a function of retention time together with the programmed gradient of mobile phase B

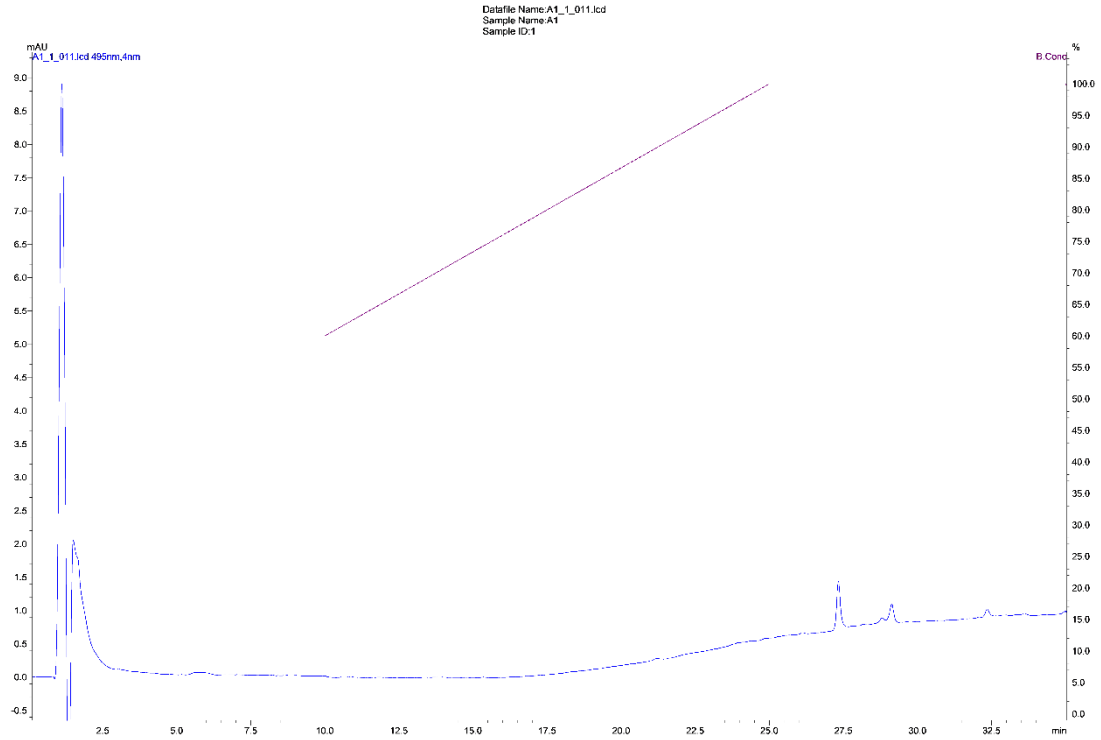


Fig. S50 Low-resolution mass spectrum of the A1 bacterial strain extract, showing the detected ions according to their m/z values and relative intensities

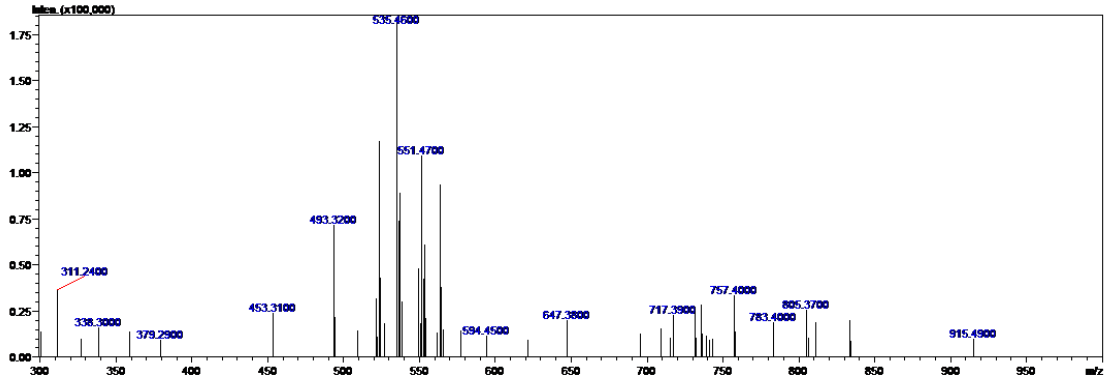


Fig. S51 High-resolution MS/MS spectrum of the precursor ion at m/z 551.5017 detected in the A1 bacterial strain extract, showing product ions at m/z 398.2320 and 299.2571

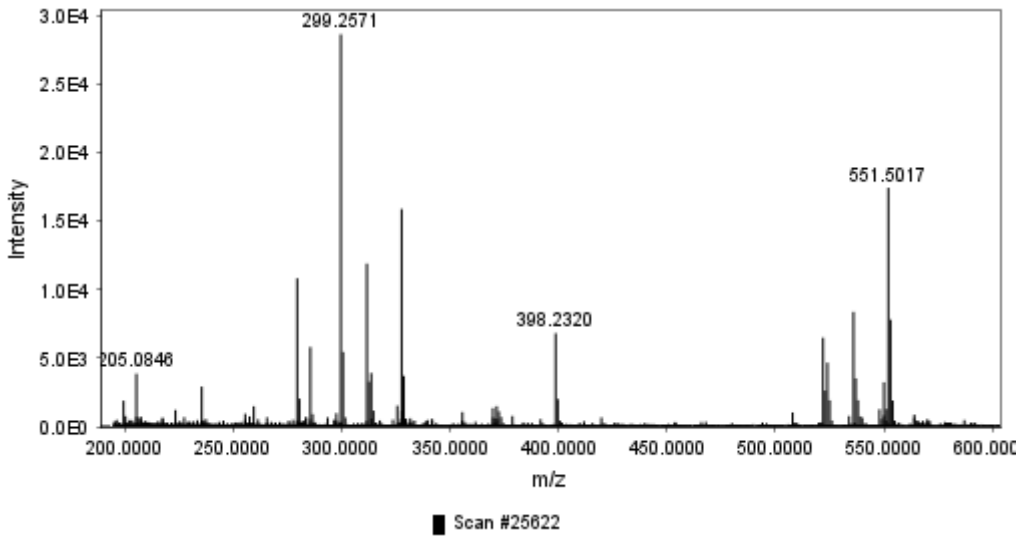


Fig. S52 High-resolution MS/MS spectrum of the precursor ion at m/z 579.5324 detected in the A1 bacterial strain extract, showing product ions at m/z 451.4506, 398.2323, and 327.2885

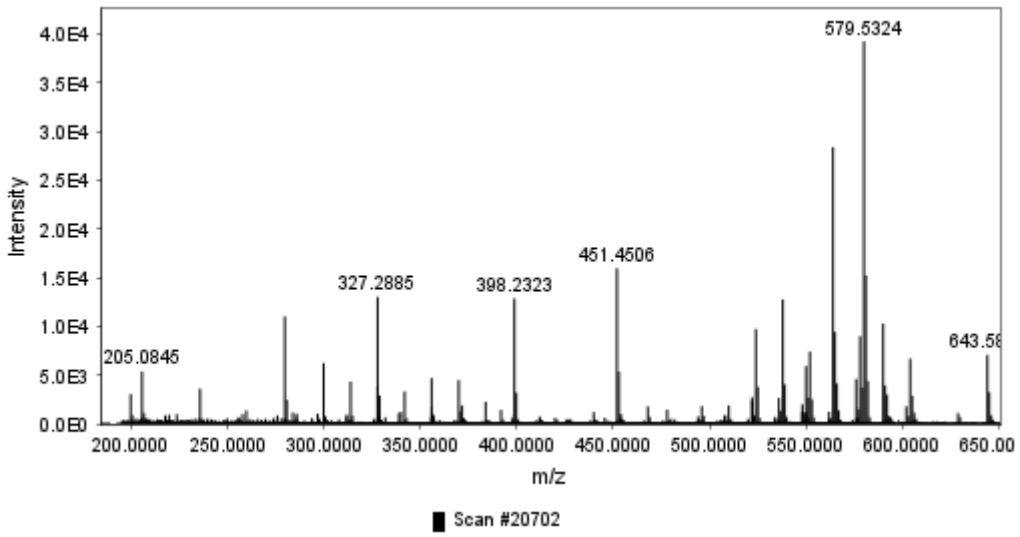


Fig. S53 High-resolution MS/MS spectrum of the precursor ion at m/z 549.4860 detected in the A1 bacterial strain extract, showing product ions at m/z 327.2887 and 398.2329

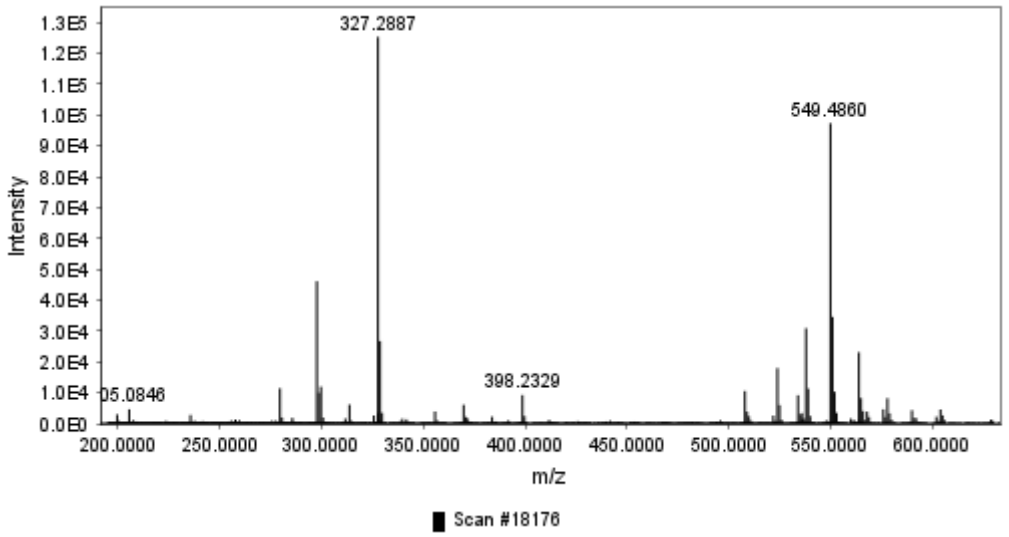


Fig. S54 High-resolution MS/MS spectrum of the precursor ion at m/z 537.4856 detected in the A1 bacterial strain extract, showing product ions at m/z 398.2315 and 299.2571

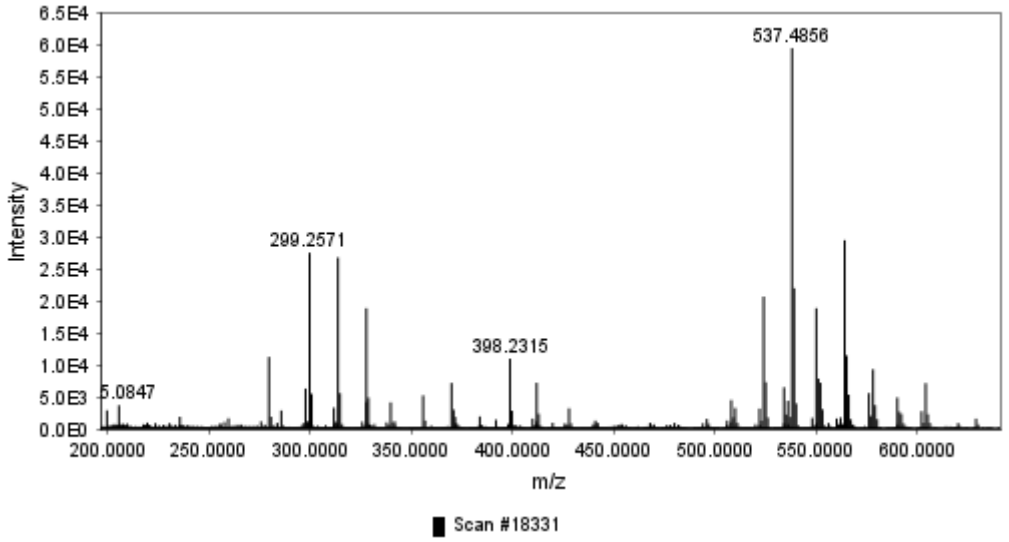


Fig. S55 High-resolution MS/MS spectrum of the precursor ion at m/z 523.4710 detected in the A1 bacterial strain extract, showing product ions at m/z 463.4145, 369.3719, and 299.2569

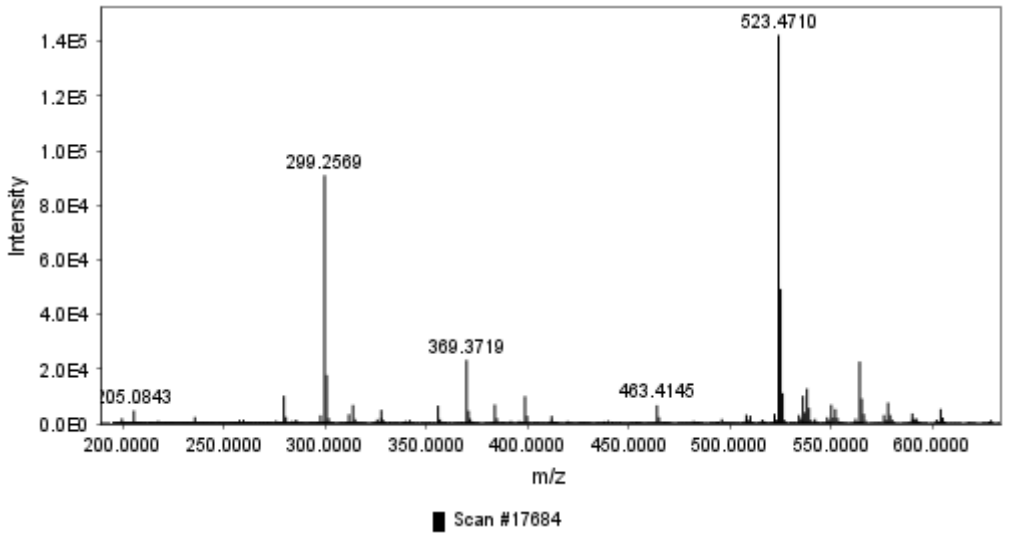


Fig. S56 High-resolution MS/MS spectrum of the precursor ion at m/z 547.4699 detected in the A1 bacterial strain extract, showing product ions at m/z 440.3982, 369.3513, and 279.1575

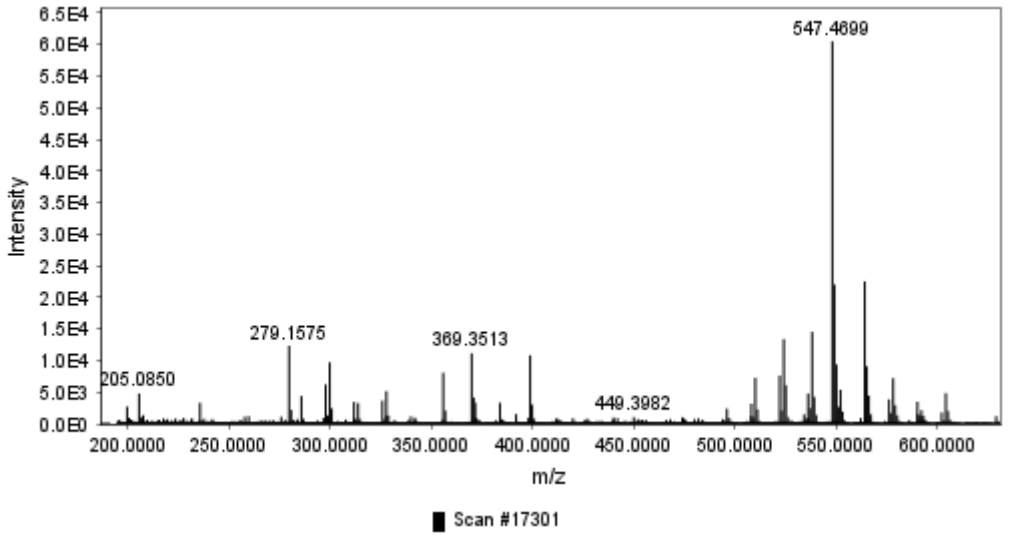


Fig. S57 High-resolution MS/MS spectrum of the precursor ion at m/z 521.4553 detected in the A1 bacterial strain extract, showing product ions at m/z 398.2329, 355.2837, and 279.1585

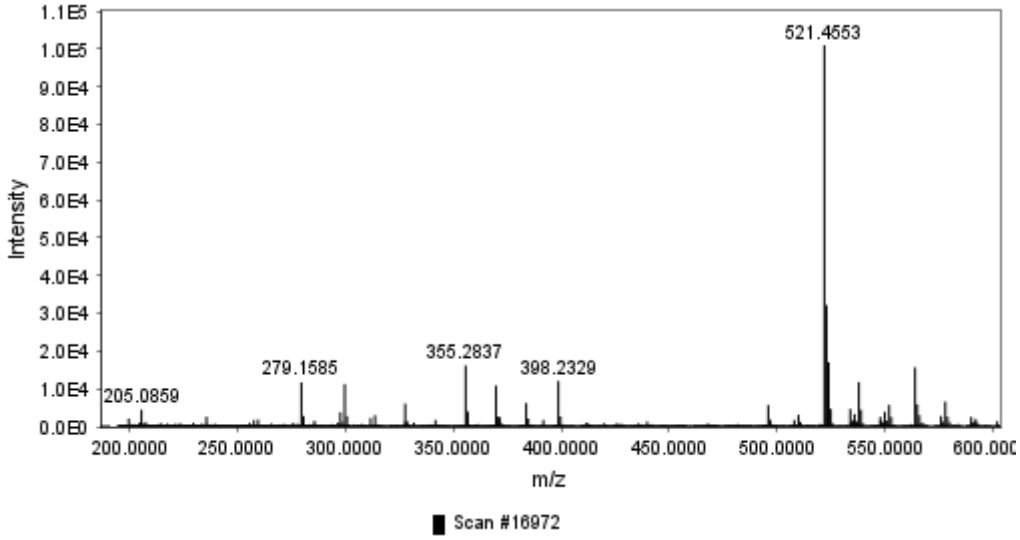


Fig. S58 High-resolution MS/MS spectrum of the precursor ion at m/z 563.5022 detected in the A1 bacterial strain extract, showing product ions at m/z 435.3825, 355.2836, and 279.1578

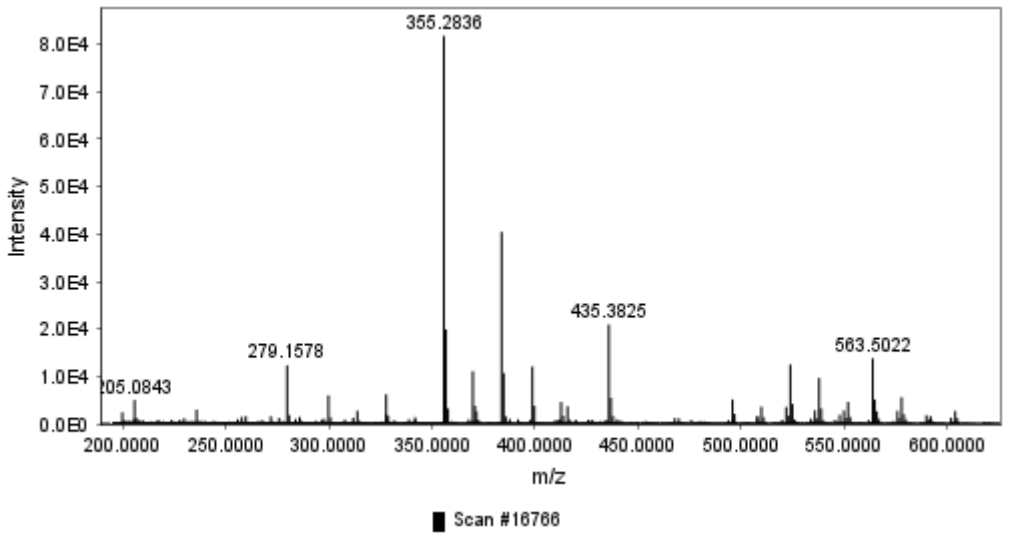
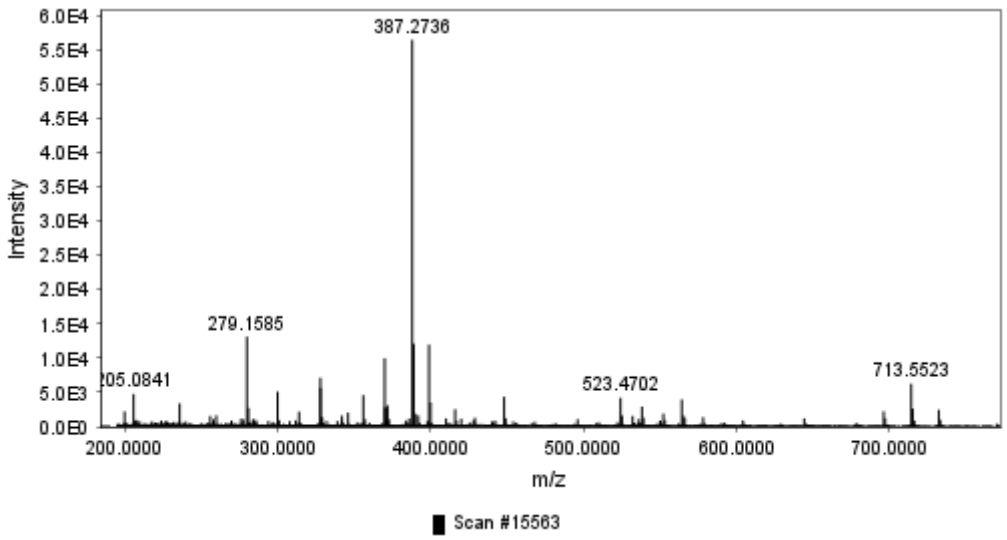


Fig. S59 High-resolution MS/MS spectrum of the precursor ion at m/z 713.5523 detected in the A1 bacterial strain extract, showing product ions at m/z 523.4702, 387.2736, and 279.1585


6.0E4
5.5E4
5.0E4
4.5E4
4.0E4
3.5E4
3.0E4
2.5E4
2.0E4
1.5E4
1.0E4
5.0E3
0.0E0
Intensity
387.2736
279.1585
205.0841
523.4702
713.5523
200.0000
300.0000
400.0000
500.0000
600.0000
700.0000
m/z
Scan #15563